Title: Daily oscillation of the excitation/inhibition ratio is disrupted in two mouse models of autism

Michelle C.D. Bridi[1], Nancy Luo[1], Grace Kim[1], Caroline O'Ferrall[2], Ruchit Patel[2], Sarah Bertrand[2], Sujatha Kannan[2], and Alfredo Kirkwood[1]

[1]Zanvyl Krieger Mind/Brain Institute, Johns Hopkins University, Baltimore, MD

[2]Department of Anesthesiology and Critical Care Medicine, Johns Hopkins University School of Medicine, Baltimore, MD

Abstract

Alterations to the balance between excitation and inhibition (E/I ratio) are postulated to underlie behavioral phenotypes in autism spectrum disorder (ASD) patients and mouse models. However, in wild type mice the E/I ratio is not constant, but instead oscillates across the 24h day. Therefore, we tested whether the E/I oscillation, rather than the overall E/I ratio, is disrupted in two ASD mouse lines: *Fmr1* KO and BTBR, models of syndromic and idiopathic ASD, respectively. The E/I ratio is dysregulated in both models, but in different ways: the oscillation is flattened in *Fmr1* KO and phase-shifted in BTBR mice. In both models these phenotypes associate with alterations in excitatory and inhibitory synaptic transmission and endocannabinoid signaling, but not with altered sleep. These findings suggest that ASD phenotypes may be produced by a mismatch of E/I to the appropriate behavioral state, rather than alterations to overall E/I levels *per se*.

Introduction

Autism spectrum disorder (ASD) is a prevalent neurodevelopmental disorder estimated to affect 1 in 54 children (Maenner et al., 2020). The core features of ASD are language deficits, social interaction deficits, and repetitive or restrictive behaviors and interests. These features are accompanied by sensory abnormalities in >90% of cases, and sensory processing differences have been reported to affect every sensory modality (reviewed in Geschwind, 2009; Robertson and Baron-Cohen, 2017). The visual system in particular is of great interest, as behavioral deficits have been tied to altered processing in the primary visual cortex (V1) of *Fmr1* knockout (KO) mice (Goel et al., 2018). Moreover, a recent analysis in humans concluded that regarding alterations in gene expression, "the primary visual cortex is the most affected region in ASD" (Berto et al., 2022).

ASD is genetically diverse, but elevation of the ratio between excitatory and inhibitory signaling (E/I ratio) in the brain has been proposed as a unifying mechanism (Rubenstein and Merzenich, 2003). Accordingly, higher E/I ratio and/or lower inhibition has been observed in sensory cortices of many ASD mouse models (Antoine et al., 2019; Banerjee et al., 2016; Bridi et al., 2017; Cellot and Cherubini, 2014; Chao et al., 2010; Gibson et al., 2008; Wallace et al., 2012; Zhang et al., 2014; Zhao and Yoshii, 2019). However, the opposite (decreased E/I ratio, increased inhibition, and/or decreased excitation) has also been reported (Dani et al., 2005; Delattre et al., 2013; Etherton et al., 2011; Harrington et al., 2016; Tabuchi et al., 2007; Unichenko et al., 2018).

One possible explanation for these opposing findings is that regulation of the E/I ratio, rather than the E/I ratio itself, is disrupted in ASD. In wild type (WT) mice, the E/I ratio in primary visual cortex (V1) changes over the course of the 24h light:dark cycle, such that it is low during the light (rest)

phase (Bridi et al., 2020). Therefore, an apparent elevation of the E/I ratio in ASD models could either be due to increased E/I at all times of day, or dysregulation (flattening or phase shift) of the E/I oscillation. However, studies that measure the E/I ratio a single time of day cannot distinguish between these possibilities.

These considerations prompted us to examine possible E/I ratio dysregulation in two ASD mouse models with disparate genetic causes: the *Fmr1* knockout (*Fmr1* KO) mouse, which models Fragile X syndrome (Bakker et al., 1994), the most frequent monogenic cause of intellectual disability and ASD in humans (Hagerman et al., 2017), and the BTBR *T+ Itpr3^{tf}/J* (BTBR) mouse, an inbred line that models idiopathic ASD (McFarlane et al., 2008; Meyza and Blanchard, 2017). We show that the E/I ratio is dysregulated in both *Fmr1* KO and BTBR mice but in different ways: the oscillation is flattened in *Fmr1* KO mice and phase-shifted in BTBR mice. Altered endocannabinoid (eCB) signaling, but not sleep architecture, corresponded to the patterns of E/I dysregulation in both lines, suggesting that eCB disruption could be a common feature across genetically diverse forms of ASD.

Materials and Methods

EXPERIMENTAL MODEL DETAILS

Animals

All procedures were approved by the Johns Hopkins University Institutional Animal Care and Use Committee. Mice were bred in-house on a 12:12 light:dark cycle (lights on at 7AM). Upon weaning, naïve mice were entrained for at least two weeks to a 12:12 light:dark cycle in custom entrainment chambers, with the timing of lights-on adjusted according to the experiment. Due to X-linkage of the *Fmr1* gene, only male *Fmr1* WT and KO mice were used. C57Bl/6J and BTBR mice of either sex were used. Littermates were distributed across experimental groups.

METHOD DETAILS

Slice Preparation

300 μm thick coronal brain slices containing V1 were prepared as described previously (Bridi et al., 2020). Briefly, slices were cut in ice-cold dissection buffer containing 212.7 mM sucrose, 5 mM KCl, 1.25 mM NaH_2PO_4, 10 mM $MgCl_2$, 0.5 mM $CaCl_2$, 26 mM $NaHCO_3$, and 10 mM dextrose, bubbled with 95% O_2/5% CO_2 (pH 7.4). Slices were transferred to normal artificial cerebrospinal fluid (similar to the dissection buffer except that sucrose was replaced by 119 mM NaCl, $MgCl_2$ was lowered to 1 mM, and $CaCl_2$ was raised to 2 mM) and incubated at 30 ˚C for 30 min and then at room temperature for at least 30 min before recording.

Whole-Cell Recording

Visualized whole-cell voltage clamp recordings were made from pyramidal neurons in L2/3 (35% depth from the pia) of V1. In slices from BTBR mice, recordings were restricted to a smaller posterior/medial region to account for the size and location of V1 in these mice (Fenlon et al., 2015; Fig. S2). Glass pipette recording electrodes (3–6 MΩ) were filled with different internal

solutions according to each experiment, all of which were adjusted to pH 7.2–7.3, 280–295 mOsm. Cells with an input resistance ≥ 150 MΩ and access resistance ≤ 25 MΩ were recorded. For all whole cell recordings, cells were discarded if these values changed more than 25% during the experiment. Data were filtered at 2 kHz and digitized at 10 kHz using Igor Pro (WaveMetrics, Portland, OR).

E/I ratio. The internal pipette solution for recording evoked EPSCs and IPSCs contained 8mM KCl, 125 mM cesium gluconate, 10 mM HEPES, 1 mM EGTA, 4mM Mg-ATP, 0.5mM Na-GTP, and 5 mM QX-314. Responses were recorded in the presence of 100 μM DL-APV . Reversal potentials for excitatory and inhibitory currents of +10 mV and -55 mV (without junction potential compensation) were used (Bridi et al., 2020). To evoke synaptic responses, a double-barrel glass stimulating pipette filled with ACSF was placed approximately 100-200 μm lateral to the recording electrode (layer 2/3 stimulation) or in the middle of the cortical thickness (layer 4 stimulation). A series of stimulations over a range of intensities was delivered, and the responses over the range of intensities producing a stable E/I ratio were used (Bridi et al., 2020).

Miniature postsynaptic current recordings. For mEPSC recordings, 1 μM TTX, 100 μM DL-APV and 2.5 μM gabazine were added to the perfusion buffer to isolate AMPAR-mediated mEPSCs. An internal pipette solution containing the following ingredients was used: 8 mM KCl, 125 mM cesium gluconate, 10 mM HEPES, 1 mM EGTA, 4 mM NaATP, and 5 mM QX-314. To record mIPSCs, 1 μM TTX, 100 μM DL-APV and 20 μM CNQX were included in the bath. The internal pipette solution contained: 8 mM NaCl, 120 mM cesium chloride, 10 mM HEPES, 2 mM EGTA, 4 mM MgATP, 0.5 mM NaGTP, and 10 mM QX-314. V_m was held at -70 mV.

Spontaneous IPSC recordings. To record sIPSCs, conditions were similar to mEPSC recording except no QX-314 was included in the internal pipette solution, V_m was held at +10 mV, and the bath contained only 10μM (+)-WIN55,212-2 (Cayman Chemical, Ann Arbor, MI), 10μM SR 141716A (Abmole, Houston, TX), or vehicle (0.1% DMSO). Slices were pre-incubated in these drugs for at least 1h prior to recording. Control and drug-treated slices were obtained from the same animal.

Polysomnography recording

Surgery. 4-5 week old mice were placed under isoflurane (1-2%) anesthesia and immobilized. A pocket was formed under the skin and a wireless transponder attached to four recording leads (model HD-X02, Data Sciences International, St. Paul, MN) was inserted into the pocket. Two EMG leads with 0.5 cm exposed wire were inserted into the cervical trapezius muscles and held in place with 5-0 silk sutures. The skull was cleaned with H_2O_2 and two holes were drilled for EEG lead placement (location posterior to bregma/lateral to the midline: 3.4mm/2.5mm and 1mm/1mm). EEG leads with 1-2 mm exposed wire were inserted into the holes to make contact with the dura and affixed with dental acrylic and cyanoacrylate glue. The wound was sutured closed and treated with triple antibiotic ointment. Mice were allowed to recover in their home cage for at least 7 days before recording. Home cages were then placed on top of telemetry receiver pads and EEG and EMG signals were captured (Data Sciences International, PhysioTel Receiver RPC-1) using Ponemah software (Data Sciences International, Version 6.40) for 3 consecutive

days on a light-dark cycle matching the vivarium environment. The EEG/EMG signal was sampled at 500 Hz.

Optical imaging of the intrinsic cortical signal

Animals were anesthetized using isoflurane in O_2 (induction: 2-3%, maintenance: 0.5-1%) supplemented with chlorprothixene (2 mg/kg i.p.). An incision was made in the scalp and lidocaine was applied to the margins. Exposed skull above V1 was covered in 3% agarose and an 8mm round glass coverslip. Surface vasculature was visualized by illuminating the area with 555nm light. Then the camera was focused 600 μm below the cortical surface and the area was illuminated with 610 nm light. A high refresh rate monitor (1024 × 768 @120 Hz; ViewSonic, Brea, CA) was aligned in the center of the mouse's visual field 25cm in front of the eyes. Visual stimuli consisted of a white horizontal bar on a black background (2° height) presented either to the entire visual field or only to the binocular visual field (-5° to +15° azimuth), moving continuously upward or downward (5 minutes per direction). Cortical signals were imaged using a Dalsa 1M30 CCD camera (Dalsa, Waterloo, Canada).

QUANTIFICATION AND STATISTICAL ANALYSIS

Whole-cell recordings

E/I ratio. Peak response amplitude at each holding potential was measured for each stimulus intensity and the ratio between the excitatory and inhibitory peak was calculated (Igor Pro). If multiple peaks were observed in the postsynaptic response, the magnitude of the first peak was used in order to limit the analysis to monosynaptic responses. If the first peak could not be clearly resolved, the cell was discarded from the analysis.

Spontaneous synaptic events. mEPSCs and mIPSCs were analyzed using the MiniAnalysis program (Synaptosoft, Decatur, GA). Only cells with root mean square (RMS) noise <2 (mEPSCs) or <4 (mIPSCs) were included in the analysis and event detection threshold was set at 3 times the RMS noise. 300 events with rise time <3 msec (mEPSCs) or <5 msec (mIPSCs) were selected for each cell to calculate frequency and amplitude. Non-overlapping events were used to construct the averaged traces. Spontaneous IPSCs were analyzed by calculating the unit charge (nA/s) with custom code (Matlab, MathWorks, Inc, Natick, MA) (Bridi et al., 2020). The baseline was calculated and subtracted for each 500 msec of recording. Charge was calculated as the integral of the baseline-subtracted signal. 3-4 minutes of recording were quantified for each cell.

Polysomnography.

Arousal stages were scored manually off-line as NREM sleep, REM sleep, and wake by a trained experimenter (MB) in 4-s epochs (SleepSign for Animal, Kissei Comtec). The percent time spent in each state, along with number and duration of bouts, was calculated. Power spectra were computed within each arousal state by performing a fast Fourier transform on the EEG signal with 0.5 Hz resolution. For each arousal state, spectra were normalized to the total EEG power (0.5-80 Hz) in that state. One B6 and one BTBR animal were included in sleep architecture analysis but excluded from spectral analysis due to differences in electrode placement.

Optical imaging of the intrinsic cortical signal

The cortical response at the stimulus frequency was extracted by Fourier analysis. Images were smoothed by a 5×5 low-pass Gaussian filter and the binocular region of interest (ROI) was defined as the 70% of pixels with the highest intensity in the ipsilateral eye map (Matlab, Mathworks, Natick, MA). The average number of pixels activated by the full visual field stimulus was calculated as a relative measure of V1 size. The ocular dominance value of each pixel in the binocular region was calculated as (contra-ipsi)/(contra+ipsi) and averaged to obtain the ODI.

Statistics

Data were analyzed with 2-tailed unpaired *t*-tests, Mann-Whitney tests, 2-way repeated measures ANOVAs with Holm-Sidak posthoc analysis, or Kruskal-Wallis with Dunn's posthoc analysis, as indicated in the figure legends (GraphPad Prism, San Diego, CA). $P<0.05$ was considered significant. In cases where data were not normally distributed (Kolmogorov-Smirnov normality test), nonparametric tests were used. Sample size is displayed in the figures as (number of cells, number of animals). Lines and error bars in all figure dot plots indicate mean and SEM.

Results

The E/I ratio is dysregulated in two mouse models of ASD.

We first determined whether the E/I ratio is dysregulated across the 24-h light/dark cycle in *Fmr1* KO mice. We measured the E/I ratio by electrically stimulating in V1 layer 2/3 and recording excitatory and inhibitory synaptic responses in pyramidal cells lateral to the stimulating electrode (Fig. 1A). We initially measured E/I at two time points: ZT0 and ZT12. As expected, in WT controls, the E/I ratio was higher at ZT0 ($t_{(51)}=3.92$, $P=0.0003$, unpaired *t* test). In contrast, the E/I ratio in *Fmr1* KO animals was not different between ZT0 and ZT12 ($U=312$, $P=0.22$, Mann-Whitney U test), consistent with E/I dysregulation. To distinguish between a phase shift or flattening of the E/I oscillation, we then included additional time points (ZT6, 18; Fig. 1A). While the E/I ratio in *Fmr1* WT animals was higher when the animal had been in the dark phase (ZT0, 18), there was no time of day effect in *Fmr1* KO animals, indicating that the E/I oscillation is flattened (Fig. 1B).

We then examined the E/I oscillation in BTBR and C57Bl/6J control mice (Fig. 1A). As expected, B6 controls exhibited a higher E/I ratio at ZT0 than at ZT12 (Fig. 1C). In contrast, the E/I ratio in the BTBR mice followed the opposite pattern, with a higher E/I ratio at ZT12 than ZT0 (Fig. 1C), indicating that the E/I ratio is intact but shifted in time.

The E/I ratio oscillates over the 24h day in the lateral (layer 2/3-2/3) circuit, but not in the feedforward (layer 4-2/3) circuit in V1 of WT mice (Bridi et al., 2020). To confirm that *Fmr1* KO and BTBR mice did not display an abnormal oscillation in this circuit, we electrically stimulated layer 4 while recording synaptic currents in layer 2/3 of V1 slices. We confirmed that the E/I ratio did not change across the day for *Fmr1* KO, *Fmr1* WT, BTBR, or B6 animals (Fig. S1). In contrast with primary somatosensory cortex (S1) (Antoine et al., 2019), there was no main effect of genotype for either ASD model in the layer 4-2/3 circuit of V1 (Fig. S1). Additionally, V1 area is reduced in BTBR mice (Fenlon et al., 2015), raising the concern that V1 function may also be abnormal. Using optical imaging *in vivo,* we confirmed that V1, although smaller, is functional

and expresses normal ocular dominance bias (Fig. S2). *Fmr1* KO mice are normal in these respects (Fig S2).

Altered sleep timing does not explain E/I dysregulation in two mouse models of ASD.

Sleep regulates the oscillation of both excitatory and inhibitory synaptic transmission over the course of the day (Bridi et al., 2020; Liu et al., 2010). Therefore, it is possible that the observed E/I dysregulation in *Fmr1* KO and BTBR mice is due to abnormal sleep timing. Indeed, decreased total sleep and decreased numbers of REM bouts during the light phase have been reported in *Fmr1* KO mice (Boone et al., 2018; Saré et al., 2017); however, no studies to date have performed round-the-clock polysomnographic recordings in *Fmr1* KO or BTBR mice. We therefore continuously recorded EEG and EMG signals in the home cage using wireless telemetry for three days. Sleep timing and architecture was grossly normal in *Fmr1* KO and BTBR mice compared to WT controls. Overall amounts of wake, non-REM (NREM) sleep, and REM sleep did not differ between *Fmr1* KO and WT or between BTBR and B6 mice (Fig. S3A). Furthermore, the distribution of time spent in each state across the day did not differ between *Fmr1* KO and WT mice (Fig. 2A). The overall pattern of sleep timing appeared normal in BTBR mice, but there was a significant interaction between genotype and time of day for wake and REM amounts (Fig 2B). However, these slight differences cannot explain the reversal of the E/I oscillation in BTBR mice, since BTBR mice slept primarily during the dark phase. We also examined sleep quality in each genotype (Fig. S3B-E). We observed significant differences in bout duration between the light and dark phases, but no differences due to genotype in *Fmr1* KO mice. BTBR mice had significantly longer REM bouts during both the light and dark phases. Number of bouts and sleep-wake transitions differed significantly between the light and dark phases but not between genotypes. There were slight but significant alterations in spectral power during sleep, most notably decreased NREM delta power in both models and increased REM theta power in BTBR mice compared to WT controls (Fig. S3E). We also observed a strong trend towards increased waking gamma power in *Fmr1* KO mice (Fig. S3F), consistent with previous reports (Goswami et al., 2019; Lovelace et al., 2018; Sinclair et al., 2017).

Both excitation and inhibition are dysregulated in two mouse models of ASD.

Our findings indicate that the E/I ratio is dysregulated across the day in two mouse models of autism. However, these data do not reveal whether excitation, inhibition, or both are responsible for this dysregulation. To determine this, we measured excitatory and inhibitory postsynaptic currents (mEPSCs, mIPSCs) in V1 layer 2/3 at ZT0 and ZT12. In *Fmr1* WT mice, mEPSC frequency was higher at ZT0 and mIPSC frequency was higher at ZT12 (Fig. 3A, B; Table S1) in accordance with previous findings (Bridi et al., 2020). In contrast, mEPSC and mIPSC frequency in *Fmr1* KO mice did not show time-of-day differences (Fig. 3A, B; Table S1), indicating that the dysregulation of the E/I ratio is caused by both excitatory and inhibitory synaptic transmission. No time-of-day differences in amplitude or recording conditions were observed for either mEPSCs or mIPSCs (Fig. 3; Table S1).

We performed the same experiment for BTBR and B6 control mice. In BTBR mice, both mEPSC and mIPSC frequency showed a pattern opposite to B6 mice: mEPSC frequency was lower (Fig. 4A) and mIPSC frequency was higher (Fig. 4B) at ZT0 than at ZT12. There were no differences in amplitude, recording conditions, or kinetics (Fig. 4, Table S2). These results demonstrate that

alterations to both excitatory and inhibitory synaptic signaling underlie the dysregulation of the E/I ratio in BTBR mice.

eCB signaling is dysregulated in BTBR mice.

Pharmacologically enhancing eCB signaling improves behavioral phenotypes in *Fmr1* KO and BTBR mice (Wei et al., 2016), suggesting that eCB signaling is abnormal in these lines. Furthermore, eCB signaling controls the daily oscillation of inhibitory transmission in WT mice, such that high levels of eCB signaling suppress inhibitory transmission during the active phase (Bridi et al., 2020). To test whether eCB dysregulation underlies the disrupted E/I oscillation in *Fmr1* KO and BTBR mice, we obtained acute brain slices at two times of day and measured spontaneous IPSCs (sIPSCs) in the presence of the eCB receptor agonist (+)-WIN 55,212-2 (WIN) or its vehicle. In *Fmr1* KO mice, WIN reduced sIPSCs at both times of day, indicating that endogenous eCB levels are low at both time points (Fig. 5A). In BTBR mice, WIN suppressed sIPSCs when inhibition is abnormally high (ZT0) but not when inhibition is low (ZT12), indicating that the eCB oscillation is intact but phase-shifted compared to WT mice (Fig. 5B). Repeating the experiment using an eCB receptor antagonist (SR141716A, SR) yielded complementary results (Fig. S4). Together, these results are consistent with a flattened and phase-shifted E/I oscillation in *Fmr1* KO and BTBR mice, respectively, that is driven in part by altered eCB signaling (Fig. S5).

Discussion

In WT mice, the E/I ratio and correlations between ionic conductances vary over the 24h day, indicating daily rearrangement of connectivity and function under normal conditions (Bridi et al., 2020; Tran et al., 2019). Therefore, it is crucial to consider neuronal dysfunction in models of neurological conditions against a backdrop of dynamic circuit properties. In this study, we show that the daily E/I oscillation is dysregulated in two mouse lines associated with ASD. The oscillation is flattened in *Fmr1* KO and phase-shifted in BTBR mice, caused by changes to both excitatory and inhibitory synaptic transmission. These changes cannot be explained by altered sleep timing, but patterns of inhibition are consistent with altered eCB signaling. Exploring how this dysregulation occurs is an important avenue for future investigation.

Implications for ASD

A prominent hypothesis in the field states that elevated E/I ratio is a common mechanism leading to the behavioral phenotypes across genetically diverse forms of ASD (Rubenstein and Merzenich, 2003). We propose to refine this viewpoint: on average, the magnitude of the E/I ratio is normal in ASD, but it is elevated/lowered at inappropriate times of day. This may result in a mismatch between E/I and brain state that causes abnormal behavioral phenotypes.

The E/I ratio oscillates in the L2/3-2/3 circuit, and is low during the light (rest) phase in WT animals (Bridi et al., 2020). Therefore, measuring the E/I ratio at a single time during the light phase predisposes studies to report an elevated E/I ratio, when there may be no overall difference, in mouse lines associated with ASD (see Fig. S5). Indeed, lower mIPSC frequency has been

reported in V1 L2/3 of *Cntnap2*-, *Tsc1-,* and *Ube3a*-deficient mice (Bridi et al., 2017; Wallace et al., 2012; Zhao and Yoshii, 2019), consistent with dysregulation. In contrast, *Fmr1* KO mice are reported to have normal mIPSC frequency and spontaneous activity in V1 L2/3 (Goel et al., 2018; Zhong et al., 2018), which may be attributable to differences in the time of day at which recordings were conducted and/or genetic background.

In WT mice, the E/I ratio also undergoes a daily oscillation in hippocampus and medial prefrontal cortex (Bridi et al., 2020), raising the possibility that E/I dysregulation may extend to other brain regions in *Fmr1* KO and BTBR mice. Consistent with this idea, the E/I ratio is elevated in CA1 of both lines (Cellot et al., 2016; Han et al., 2014; Sabanov et al., 2017; Wahlstrom-Helgren and Klyachko, 2015).

The E/I ratio oscillation occurs in multiple brain regions, but only in specific circuits. In WT mice, the E/I ratio in V1 oscillates daily in the layer 2/3→2/3 pathway, but not in the layer 4→2/3 pathway (Fig. 1, S1; Bridi et al., 2020). Here, we show that the E/I ratio remains is also fixed in the layer 4-2/3 circuit of both *Fmr1* KO and BTBR mice. Notably, we did not observe a general elevation of the E/I ratio in this pathway in either line (Fig. S1). This raises the possibility that pathways in which the E/I ratio is dynamically regulated are more likely to be affected in ASD models. However, we note that in S1 of *Fmr1* KO mice, the E/I ratio is elevated in the layer 4→2/3 pathway (Antoine et al., 2019). Whether these discrepancies are due to E/I oscillations occurring in different circuits in S1 and V1 remains to be determined.

Candidate Mechanisms of E/I dysregulation

One intriguing implication of our findings is that regulation of excitatory and inhibitory synaptic transmission go hand-in-hand, since they are jointly dysregulated in both *Fmr1* KO and BTBR mice. This may occur via a central mechanism controlling both excitation and inhibition, or by the dependence of excitation on inhibition (or vice versa). While the exact mechanisms remain to be elucidated, changes in mE/IPSC frequency are consistent with formation/elimination of synapses across the 24h day, implicating a number of potential candidate mechanisms.

Four moving parts comprise the E/I ratio oscillation in WT mice: increased excitation/decreased inhibition during the active phase, and decreased excitation/increased inhibition during the rest phase (Bridi et al., 2020). During the active phase, LTP has been implicated in increased excitatory transmission, and eCB signaling controls decreased inhibitory transmission (Bridi et al., 2020; Vyazovskiy et al., 2008). During the rest phase, sleep is required for decreased excitation and increased inhibition (Bridi et al., 2020; Liu et al., 2010). The ways in which these mechanisms operate in WT mice remain poorly understood, limiting our ability to interpret the exact mechanisms of dysregulation in *Fmr1* KO and BTBR mice. Nevertheless, we examined how two of these mechanisms, sleep and eCB signaling, relate to E/I dysregulation in these lines.

Sleep disruption is a common feature of autism (reviewed in Schreck and Richdale, 2020). However, despite a variety of altered sleep and activity characteristics, a grossly normal nocturnal activity pattern in preserved across many commonly used ASD-related mouse lines, including *Fmr1* KO (Angelakos et al., 2017; Colas et al., 2005; Ehlen et al., 2015; El Helou et al., 2013; Ingiosi et al., 2019; Li et al., 2015; Lipton et al., 2017; Liu et al., 2017; Lu et al., 2019; Saré et al., 2021, 2017; Seok et al., 2018; Thomas et al., 2017; Tsuchiya et al., 2015; Wither et al., 2012; Zhang et al., 2008). Here we confirmed that sleep timing follows a normal pattern of nocturnal

activity in *Fmr1* KO and BTBR mice, but did not replicate the REM sleep deficit reported in *Fmr1* KO mice (Boone et al., 2018), possibly due to the longer recording sessions used in our study, or an emergence of the deficit with age (Saré et al., 2017). Therefore, dysregulation is unlikely to arise from altered sleep timing in *Fmr1* KO or BTBR mice, and in ASD model mice more broadly. However, NREM delta power was reduced in both genotypes, consistent with reports in other ASD-related mouse lines (Angelakos et al., 2017; Ehlen et al., 2015; Ingiosi et al., 2019; Johnston et al., 2014; Liu et al., 2017; Lu et al., 2019), suggesting that altered NREM sleep quality could contribute to E/I dysregulation.

Altered eCB signaling has also been implicated in ASD in humans (Aran et al., 2019; Pretzsch et al., 2019), as well as in *Fmr1* KO, BTBR, *Nlgn*3^{R451C}, and *Nlgn3* KO mice (Busquets-Garcia et al., 2013; Földy et al., 2013; Gomis-González et al., 2016; Jung et al., 2012; Maccarrone et al., 2010; Qin et al., 2015; Speed et al., 2015; Wei et al., 2016; Zhang and Alger, 2010). Here, we report that inhibitory transmission is susceptible to manipulations of eCB signaling in *Fmr1* KO and BTBR mice (Fig. 5, S4), indicating that eCB signaling pathways are intact. However, the response eCB manipulation is flattened in *Fmr1* KO and shifted in time compared to WT mice (Bridi et al., 2020), suggesting that altered timing of eCB release underlies the dysregulation of inhibition in both lines.

An additional candidate mechanism is glial function. Microglia and astrocytes play a role in pruning and function of excitatory and inhibitory synapses (Blinzinger and Kreutzberg, 1968; Chung et al., 2013; Favuzzi et al., 2021; Lee et al., 2021; Oliet et al., 2001; Paolicelli et al., 2011; Shigetomi et al., 2012), thus shaping connectivity in the cortex (Liu et al., 2021). Importantly, microglial and astrocyte function, which in WT mice depend on arousal state (Bellesi et al., 2017; Ding et al., 2013; Ingiosi et al., 2020; Liu et al., 2019; Paukert et al., 2014; Stowell et al., 2019), is altered in both *Fmr1* KO and mice BTBR mice (Eissa et al., 2020; van der Goot et al., 2019; Heo et al., 2011; Higashimori et al., 2013; Jawaid et al., 2018).

Consequences of dysregulated E/I balance

The exact behavioral impact of altered E/I balance in ASD remains largely unclear. A common view states that network hyperexcitability associated with reduced inhibition and altered inhibitory plasticity impairs neural processing (for recent reviews see Antoine, 2022; Chen et al., 2022; Ferguson and Gao, 2018; Liu et al., 2022), an idea well suited to account for perceptual learning deficits resulting from impairments in sensory discrimination (Goel et al., 2018). Alternatively, it has been proposed that altered excitatory and inhibitory synaptic transmission may not be a primary effect of the ASD phenotype, but rather reflect homeostatic compensations that mitigate other types of dysfunction (Antoine et al., 2019; Domanski et al., 2019; Nelson and Valakh, 2015). E/I dysregulation might offer unique opportunities to discriminate between these two possibilities because E/I differences between mutant and WT animals will vary in magnitude and sign across the day. In these cases, circadian-like variations in the degree of behavioral impairments, as reported recently (Sawicka et al., 2019), correlating with daily E/I discrepancies will support a direct impact of altered E/I on behavioral phenotype.

Conclusions.

The E/I ratio is dynamically regulated, likely via multiple mechanisms acting in concert. Each of these mechanisms has the potential to be affected by a variety of genetic and environmental factors, making the E/I oscillation vulnerable to disruption. Therefore, E/I dysregulation may be a point of convergence for genetically diverse forms of ASD, ultimately resulting in common behavioral phenotypes. Further exploring the underlying mechanisms will provide crucial insight to the pathophysiology of ASD.

FIGURE LEGENDS:

Figure 1. E/I is dysregulated in two mouse models of autism. (A) Left: *Fmr1* KO/WT (green) and BTBR/B6 (blue) mice were sacrificed at the indicated times of day. Right: Acute brain slices containing V1 were obtained, and responses to layer 2/3 stimulation over a range of intensities were recorded using whole-cell patch clamp of layer 2/3 pyramidal neurons. Inhibitory (upward deflection) and excitatory (downward deflection) responses were recorded in the same cell and the E/I ratio was calculated using the stimulation intensities over which the E/I ratio was stable (Bridi et al., 2020). (B) Oscillation of the E/I ratio across the day is absent in *Fmr1* KO mice. Top: *Fmr1* KO Kruskal-Wallis $H_{(3, 102)}$=1.62, P=0.65. Bottom: *Fmr1* WT 1-way ANOVA $F_{(3, 94)}$=6.67, P=0.0004; Holm-Sidak post-hoc test P values indicated. (C) BTBR mice exhibit a phase-shifted E/I oscillation, such that the E/I ratio is high at ZT12, contrasting with higher E/I at ZT0 in B6 mice. Top: BTBR 2-tailed t test $t_{(45)}$=2.64; Bottom: B6 2-tailed t test $t_{(41)}$=2.93. For all panels, sample size is indicated as (cells, mice). Error bars indicate mean±SEM. Example traces are normalized to peak inhibitory response.

Figure 2. Sleep timing is normal in *Fmr1* KO and BTBR mice. (A) Percent time *Fmr1* mice spent awake (A_1), in NREM sleep (A_2), and in REM sleep (A_3). There was no significant main effect of genotype for any arousal state (%W $F_{(1, 12)}$=3.43, P=0.09, %NREM $F_{(1, 12)}$=2.80, P=0.12, %REM $F_{(1, 12)}$=0.86, P=0.37). There was also no significant genotype × time of day interaction when data were broken into 1h bins (left) (%W $F_{(23, 276)}$=0.88, P=0.63, %NREM $F_{(23, 276)}$=0.88, P=0.63, %REM $F_{(23, 276)}$=0.76, P=0.78) or averaged across the 12-h light and dark phases (right) (%W $F_{(1, 12)}$=3.12, P=0.10, %NREM $F_{(1, 12)}$=3.23, P=0.09, %REM $F_{(1, 12)}$=1.81, P=0.20). There was a significant main effect of time for all states (%W: $F_{(1, 12)}$=153.0, P<0.0001; %NREM: $F_{(1, 12)}$=162.9, P<0.0001; %REM: $F_{(1, 12)}$=85.6, P<0.0001). (B) Percent time BTBR and B6 mice spent in each arousal state. BTBR mice displayed grossly normal sleep timing (i.e. slept more during the dark phase) and there was no significant main effect of genotype for any arousal state (%W $F_{(1, 14)}$=0.72, P=0.41, %NREM $F_{(1, 14)}$=0.48, P=0.50, %REM $F_{(1, 14)}$=0.54, P=0.47). There were small but significant interaction effects for wake (B_1) and REM sleep (B_3) when data were broken into 1h bins (left) (%W $F_{(23, 322)}$=1.57, P=0.048, %NREM $F_{(23,322)}$=1.521, P=0.06, %REM $F_{(23, 322)}$=2.05, P=0.0035) and for REM sleep (B_3) when data were averaged into 12h bins (right) (%W $F_{(1, 14)}$=2.39, P=0.24, %NREM $F_{(1, 14)}$=1.95, P=0.18, %REM $F_{(1, 14)}$=4.93, P=0.04). There was a main time of day effect for all states (%W $F_{(1, 14)}$=258.9, P<0.0001, %NREM $F_{(1, 14)}$=232.0, P<0.0001, %REM $F_{(1, 14)}$=342.5, P<0.0001). Data were averaged over 3 recording days for each mouse prior to statistical analysis. All data were analyzed using 2-way repeated measures ANOVAs. Data are shown as mean ± SEM. N=number of mice.

Figure 3. Oscillation of both excitation and inhibition is flattened in *Fmr1* KO mice. (A) mEPSC frequency does not change with time of day in *Fmr1* KO mice (U=613, P=0.35, Mann-Whitney test), but is higher at ZT0 in *Fmr1* WT control mice (U=269, P=0.001, Mann-Whitney test). Amplitude did not change with time of day in either genotype (KO: U=579, P=0.19; WT: U=445, P=0.39; Mann-Whitney test). (B) mIPSC frequency does not change with time of day in *Fmr1* KO mice (U=596, P=0.93, Mann-Whitney test), but is higher at ZT12 in *Fmr1* WT control mice ($t_{(51)}$=2.69, P=0.0098, t test). Amplitude did not change with time of day in either genotype (KO: $t_{(68)}$=1.26, P=0.21; WT: $t_{(51)}$=0.46, P=0.65, t test). Data are presented as mean±SEM. Sample size is indicated as (cells, mice). Averaged traces: solid lines indicate ZT0, dotted lines indicate ZT12; scaled, superimposed averaged traces illustrate that there was no difference in kinetics between the two times of day (Table S1).

Figure 4. Oscillation of both excitation and inhibition is reversed in BTBR mice. (A) mEPSC frequency is higher at ZT12 in BTBR mice (U=322, P=0.016, Mann-Whitney test), and higher at ZT0 in B6 control mice ($t_{(67)}$=2.53, P=0.014, t test). Amplitude did not change with time of day in either genotype (BTBR: $t_{(61)}$=1.08, P=0.28; B6: $t_{(67)}$=0.11, P=0.91; t test). (B) mIPSC frequency is higher at ZT0 in BTBR mice (U=278, P=0.026, Mann-Whitney test), and higher at ZT12 in B6 controls (U=464, P=0.017, Mann-Whitney test). Amplitude did not change with time of day in either genotype (BTBR: $t_{(56)}$=0.93, P=0.36; B6: $t_{(72)}$=1.71, P=0.09, t test). Data are presented as mean±SEM. Sample size is indicated as (cells, mice). Averaged traces: solid lines indicate ZT0, dotted lines indicate ZT12; scaled, superimposed averaged traces illustrate that there was no difference in kinetics between the two times of day (Table S2).

Figure 5. eCB signaling is dysregulated in *Fmr1* KO and BTBR mice. Slices were obtained at ZT0 or ZT12 and incubated in the eCB agonist WIN (10μM) or vehicle. sIPSCs were recorded from both treatment conditions in each animal. (A) Example traces (top) and quantification (bottom) of sIPSCs recorded from *Fmr1* KO slices. WIN significantly decreased sIPSC charge at both ZT0 and ZT12 (ANOVA on ranks H=28.73, P<0.0001; P values indicate significant differences according to Dunn's post-hoc test). sIPSC charge did not differ between times of day within vehicle or WIN treatment groups (P>0.9999). (B) Example traces (top) and quantification (bottom) of sIPSCs recorded from BTBR slices. WIN suppressed inhibitory transmission only at ZT0 (Kruskal-Wallis ANOVA on ranks H=16.9, P=0.0007; P values indicate significant differences between groups according to Dunn's post-hoc test). Data are shown as mean ±SEM and sample size is indicated as (cells, mice).

REFERENCES

Angelakos, C.C., Watson, A.J., O'Brien, W.T., Krainock, K.S., Nickl-Jockschat, T., and Abel, T. (2017). Hyperactivity and male-specific sleep deficits in the 16p11.2 deletion mouse model of autism. Autism Res *10*, 572–584. DOI: 10.1002/aur.1707.

Antoine, M.W. (2022). Paradoxical hyperexcitability in disorders of neurodevelopment. Front Mol Neurosci *15*, 826679. DOI: 10.3389/fnmol.2022.826679.

Antoine, M.W., Langberg, T., Schnepel, P., and Feldman, D.E. (2019). Increased excitation-inhibition ratio stabilizes synapse and circuit excitability in four autism mouse models. Neuron *101*, 648–661. DOI: 10.1016/j.neuron.2018.12.026.

Aran, A., Eylon, M., Harel, M., Polianski, L., Nemirovski, A., Tepper, S., Schnapp, A., Cassuto, H., Wattad, N., and Tam, J. (2019). Lower circulating endocannabinoid levels in children with autism spectrum disorder. Mol Autism *10*, 1–11. DOI: 10.1186/s13229-019-0256-6.

Bakker, C.E., Verheij, C., Willemsen, R., van der Helm, R., Oerlemans, F., Vermey, M., Bygrave, A., Hoogeveen, A.T., Oostra, B.A., Reyniers, E., et al. (1994). Fmr1 knockout mice : A model to study fragile X mental retardation. Cell *78*, 23–33. DOI: 10.1016/0092-8674(94)90569-X.

Banerjee, A., Rikhye, R. V, Breton-Provencher, V., Tang, X., Li, C., Li, K., Runyan, C.A., Fu, Z., Jaenisch, R., and Sur, M. (2016). Jointly reduced inhibition and excitation underlies circuit-wide changes in cortical processing in Rett syndrome. Proc Natl Acad Sci USA *113*, E7287–E7296. DOI: 10.1073/pnas.1615330113.

Bellesi, M., de Vivo, L., Chini, M., Gilli, F., Tononi, G., and Cirelli, C. (2017). Sleep loss promotes astrocytic phagocytosis and microglial activation in mouse cerebral cortex. J Neurosci *37*, 5263–5273. DOI: 10.1523/JNEUROSCI.3981-16.2017.

Berto, S., Treacher, A.H., Caglayan, E., Luo, D., Haney, J.R., Gandal, M.J., Geschwind, D.H., Montillo, A.A., and Konopka, G. (2022). Association between resting-state functional brain connectivity and gene expression is altered in autism spectrum disorder. Nat Commun *13*, 3328. DOI: 10.1038/s41467-022-31053-5.

Blinzinger, K., and Kreutzberg, G. (1968). Displacement of synaptic terminals from regenerating motoneurons by microglial cells. Zeitschrift Fur Zellforsch *85*, 145–157. DOI: 10.1007/BF00325030.

Boone, C.E., Davoudi, H., Harrold, J.B., and Foster, D.J. (2018). Abnormal sleep architecture and hippocampal circuit dysfunction in a mouse model of fragile X syndrome. Neuroscience *384*, 275–289. DOI: 10.1016/j.neuroscience.2018.05.012.

Bridi, M.C.D., Zong, F.-J., Min, X., Luo, N., Tran, T., Qiu, J., Severin, D., Zhang, X.-T., Wang, G., Zhu, Z.-J., et al. (2020). Daily oscillation of the excitation-inhibition balance in visual cortical circuits. Neuron *105*, 621–629. DOI: 10.1016/j.neuron.2019.11.011.

Bridi, M.S., Park, S.M., and Huang, S. (2017). Developmental disruption of GABAAR-meditated inhibition in Cntnap2 KO mice. ENeuro *4*, e0162–17.2017. DOI: 10.1523/ENEURO.0162-17.2017.

Busquets-Garcia, A., Gomis-González, M., Guegan, T., Agustín-Pavón, C., Pastor, A., Mato, S., Pérez-Samartín, A., Matute, C., de la Torre, R., Dierssen, M., et al. (2013). Targeting the endocannabinoid system in the treatment of fragile X syndrome. Nat Med *19*, 603–607. DOI:

10.1038/nm.3127.

Cellot, G., and Cherubini, E. (2014). Reduced inhibitory gate in the barrel cortex of Neuroligin3 R451C knock-in mice , an animal model of autism spectrum disorders. Physiol Rep *2*, e12077. DOI: 10.14814/phy2.12077.

Cellot, G., Maggi, L., Di Castro, M.A., Catalano, M., Migliore, R., Migliore, M., Scattoni, M.L., Calamandrei, G., and Cherubini, E. (2016). Premature changes in neuronal excitability account for hippocampal network impairment and autistic-like behavior in neonatal BTBR T+tf/J mice. Sci Rep *6*, 31696. DOI: 10.1038/srep31696.

Chao, H.-T., Chen, H., Samaco, R.C., Xue, M., Chahrour, M., Yoo, J., Neul, J.L., Gong, S., Lu, H., Heintz, N., et al. (2010). Dysfunction in GABA signalling mediates autism-like stereotypies and Rett syndrome phenotypes. Nature *468*, 263–296. DOI: 10.1038/nature09582.

Chen, L., Li, X., Tjia, M., and Thapliyal, S. (2022). Homeostatic plasticity and excitation-inhibition balance: The good, the bad, and the ugly. Curr Opin Neurobiol *75*, 102553. DOI: 10.1016/j.conb.2022.102553.

Chung, W.-S., Clarke, L.E., Wang, G.X., Stafford, B.K., Sher, A., Chakraborty, C., Joung, J., Foo, L.C., Thompson, A., Chen, C., et al. (2013). Astrocytes mediate synapse elimination through MEGF10 and MERTK pathways. Nature *504*, 394–400. DOI: 10.1038/nature12776.

Colas, D., Wagstaff, J., Fort, P., Salvert, D., and Sarda, N. (2005). Sleep disturbances in Ube3a maternal-deficient mice modeling Angelman syndrome. Neurobiol Dis *20*, 471–478. DOI: 10.1016/j.nbd.2005.04.003.

Dani, V.S., Chang, Q., Maffei, A., Turrigiano, G.G., Jaenisch, R., and Nelson, S.B. (2005). Reduced cortical activity due to a shift in the balance between excitation and inhibition in a mouse model of Rett Syndrome. Proc Natl Acad Sci U S A *102*, 12560–12565. DOI: 10.1073/pnas.0506071102.

Delattre, V., La Mendola, D., Meystre, J., Markram, H., and Markram, K. (2013). Nlgn4 knockout induces network hypo-excitability in juvenile mouse somatosensory cortex in vitro. Sci Rep *3*, 2897. DOI: 10.1038/srep02897.

Ding, F., Donnell, J.O., Thrane, A.S., Zeppenfeld, D., Kang, H., Xie, L., Wang, F., and Nedergaard, M. (2013). a1-Adrenergic receptors mediate coordinated Ca2+ signaling of cortical astrocytes in awake, behaving mice. Cell Calcium *54*, 387–394. DOI: 10.1016/j.ceca.2013.09.001.

Domanski, A.P.F., Booker, S.A., Wyllie, D.J.A., Isaac, J.T.R., and Kind, P.C. (2019). Cellular and synaptic phenotypes lead to disrupted information processing in Fmr1-KO mouse layer 4 barrel cortex. Nat Commun *10*, 4814. DOI: 10.1038/s41467-019-12736-y.

Ehlen, J.C., Jones, K.A., Pinckney, L., Gray, C.L., Burette, S., Weinberg, R.J., Evans, J.A., Brager, A.J., Zylka, M.J., Paul, K.N., et al. (2015). Maternal Ube3a loss disrupts sleep homeostasis but leaves circadian rhythmicity largely intact. J Neurosci *35*, 13587–13598. DOI: 10.1523/JNEUROSCI.2194-15.2015.

Eissa, N., Jayaprakash, P., Stark, H., Łazewska, D., Kiec-Kononowicz, K., and Sadek, B. (2020). Simultaneous blockade of histamine H3 receptors and inhibition of acetylcholine esterase alleviate autistic-like behaviors in BTBR T + tf/J mouse model of autism. Biomolecules *10*, 1251. DOI: 10.3390/biom10091251.

Etherton, M., Földy, C., Sharma, M., Tabuchi, K., Liu, X., Shamloo, M., Malenka, R.C., and

Sudhof, T.C. (2011). Autism-linked neuroligin-3 R451C mutation differentially alters hippocampal and cortical synaptic function. Proc Natl Acad Sci U S A *108*, 13764–13769. DOI: 10.1073/pnas.1111093108.

Favuzzi, E., Huang, S., Saldi, G.A., Binan, L., Ibrahim, L.A., Fernandez-Otero, M., Cao, Y., Zeine, A., Sefah, A., Zheng, K., et al. (2021). GABA-receptive microglia selectively sculpt developing inhibitory circuits. Cell *184*, 4048–4063. DOI: 10.1016/j.cell.2021.06.018.

Fenlon, L.R., Liu, S., Gobius, I., Kurniawan, N.D., Murphy, S., Moldrich, R.X., and Richards, L.J. (2015). Formation of functional areas in the cerebral cortex is disrupted in a mouse model of autism spectrum disorder. Neural Dev *10*, 10. DOI: 10.1186/s13064-015-0033-y.

Ferguson, B.R., and Gao, W.-J. (2018). PV interneurons : Critical regulators of E/I balance for prefrontal cortex-dependent behavior and psychiatric disorders. Front Neural Circuits *12*, 37. DOI: 10.3389/fncir.2018.00037.

Földy, C., Malenka, R.C., and Sudhof, T.C. (2013). Autism-associated neuroligin-3 mutations commonly disrupt tonic endocannabinoid signaling. Neuron *78*, 498–509. DOI: 10.1016/j.neuron.2013.02.036.

Geschwind, D.H. (2009). Advances in autism. Annu Rev Med *60*, 367–380. DOI: 10.1146/annurev.med.60.053107.121225.

Gibson, J.R., Bartley, A.F., Hays, S.A., and Huber, K.M. (2008). Imbalance of neocortical excitation and inhibition and altered UP states reflect network hyperexcitability in the mouse model of fragile X syndrome. J Neurophysiol *100*, 2615–2626. DOI: 10.1152/jn.90752.2008.

Goel, A., Cantu, D.A., Guilfoyle, J., Chaudhari, G.R., Newadkar, A., Todisco, B., de Alba, D., Kourdougli, N., Schmitt, L.M., Pedapati, E., et al. (2018). Impaired perceptual learning in a mouse model of Fragile X syndrome is mediated by parvalbumin neuron dysfunction and is reversible. Nat Neurosci *21*, 1404–1411. DOI: 10.1038/s41593-018-0231-0.

Gomis-González, M., Busquets-Garcia, A., Matute, C., Maldonado, R., Mato, S., and Ozaita, A. (2016). Possible therapeutic doses of cannabinoid type 1 receptor antagonist reverses key alterations in fragile X syndrome mouse model. Genes (Basel) *7*, 56. DOI: 10.3390/genes7090056.

van der Goot, E., Bruinenberg, V.M., Hormann, F.M., Eisel, U.L.M., van Spronsen, F.J., and Van der Zee, E.A. (2019). Hippocampal microglia modifications in C57Bl/6 Pah enu2 and BTBR Pah enu2 phenylketonuria (PKU) mice depend on the genetic background , irrespective of disturbed sleep patterns. Neurobiol Learn Mem *160*, 139–143. DOI: 10.1016/j.nlm.2018.05.002.

Goswami, S., Cavalier, S., Sridhar, V., Huber, K.M., and Gibson, J.R. (2019). Local cortical circuit correlates of altered EEG in the mouse model of Fragile X syndrome. Neurobiol Dis *124*, 563–572. DOI: 10.1016/j.nbd.2019.01.002.

Hagerman, R.J., Berry-Kravis, E., Hazlett, H.C., Bailey, D.B.J., Moine, H., Kooy, R.F., Tassone, F., Gantois, I., Sonenberg, N., Mandel, J.L., et al. (2017). Fragile X syndrome. Nat Rev Dis Prim *3*, 17065. DOI: 10.1038/nrdp.2017.65.

Han, S., Tai, C., Jones, C.J., Scheuer, T., and Catterall, W.A. (2014). Enhancement of inhibitory neurotransmission by GABAA receptors having α2,3 -subunits ameliorates behavioral deficits in a mouse model of autism. Neuron *81*, 1282–1289. DOI: 10.1016/j.neuron.2014.01.016.

Harrington, A.J., Raissi, A., Rajkovich, K., Berto, S., Kumar, J., Molinaro, G., Raduazzo, J., Guo, Y., Loerwald, K., Konopka, G., et al. (2016). MEF2C regulates cortical inhibitory and excitatory

synapses and behaviors relevant to neurodevelopmental disorders. Elife *5*, e20059. DOI: 10.7554/eLife.20059.

El Helou, J., Bélanger-nelson, E., Freyburger, M., Dorsaz, S., and Curie, T. (2013). Neuroligin-1 links neuronal activity to sleep-wake regulation. Proc Natl Acad Sci USA *110*, 9974–9979. DOI: 10.1073/pnas.1221381110/-/DCSupplemental.www.pnas.org/cgi/doi/10.1073/pnas.1221381110.

Heo, Y., Zhang, Y., Gao, D., Miller, V.M., and Lawrence, D.A. (2011). Aberrant immune responses in a mouse with behavioral disorders. PLoS One *6*, e20912. DOI: 10.1371/journal.pone.0020912.

Higashimori, H., Morel, L., Huth, J., Lindemann, L., Dulla, C., Taylor, A., Freeman, M., and Yang, Y. (2013). Astroglial FMRP-dependent translational down-regulation of mGluR5 underlies glutamate transporter GLT1 dysregulation in the fragile X mouse. Hum Mol Genet *22*, 2041–2054. DOI: 10.1093/hmg/ddt055.

Ingiosi, A.M., Schoch, H., Wintler, T., Singletary, K.G., Righelli, D., Roser, L.G., Medina, E., Risso, D., Frank, M.G., and Peixoto, L. (2019). Shank3 modulates sleep and expression of circadian transcription factors. Elife *8*, e42819. DOI: 10.7554/eLife.42819.

Ingiosi, A.M., Hayworth, C.R., Harvey, D.O., Singletary, K.G., Rempe, M.J., Wisor, J.P., and Frank, M.G. (2020). A role for astroglial calcium in mammalian sleep and sleep regulation. Curr Biol *30*, 4373–4383. DOI: 10.1016/j.cub.2020.08.052.

Jawaid, S., Kidd, G.J., Wang, J., Swetlik, C., Dutta, R., and Trapp, B.D. (2018). Alterations in CA1 hippocampal synapses in a mouse model of Fragile X Syndrome. Glia *66*, 789–800. DOI: 10.1002/glia.23284.

Johnston, M. V, Ammanuel, S., O'Driscoll, C., Wozniak, A., Naidu, S., and Kadam, S.D. (2014). Twenty-four hour quantitative-EEG and in-vivo glutamate biosensor detects activity and circadian rhythm dependent biomarkers of pathogenesis in Mecp2 null mice. Front Sytems Neurosci *8*, 1–13. DOI: 10.3389/fnsys.2014.00118.

Jung, K.-M., Sepers, M., Henstridge, C.M., Lassalle, O., Neuhofer, D., Martin, H., Ginger, M., Frick, A., DiPatrizio, N. V, Mackie, K., et al. (2012). Uncoupling of the endocannabinoid signalling complex in a mouse model of fragile X syndrome. Nat Commun *3*, 1080. DOI: 10.1038/ncomms2045.

Lee, J.-H., Kim, J., Noh, S., Lee, H., Lee, S.Y., Mun, J.Y., Park, H., and Chung, W. (2021). Astrocytes phagocytose adult hippocampal synapses for circuit homeostasis. Nature *590* DOI: 10.1038/s41586-020-03060-3.

Li, Q., Loh, D.H., Kudo, T., Truong, D., Derakhshesh, M., Macdowell, Z., Ghiani, C.A., Tsoa, R., Cheng, Y., Sun, Y.E., et al. (2015). Circadian rhythm disruption in a mouse model of Rett syndrome circadian disruption in RTT. Neurobiol Dis *77*, 155–164. DOI: 10.1016/j.nbd.2015.03.009.

Lipton, J.O., Boyle, L.M., Yuan, E.D., Hochstrasser, K.J., Chifamba, F.F., Nathan, A., Tsai, P.T., Davis, F., and Sahin, M. (2017). Aberrant proteostasis of BMAL1 underlies circadian abnormalities in a paradigmatic mTOR-opathy. Cell Rep *20*, 868–880. DOI: 10.1016/j.celrep.2017.07.008.

Liu, J.J., Grace, K.P., Horner, R.L., Cortez, M.A., Shao, Y., and Jia, Z. (2017). Neuroligin 3 R451C mutation alters electroencephalography spectral activity in an animal model of autism

spectrum disorders. Mol Brain *10*, 10. DOI: 10.1186/s13041-017-0290-2.

Liu, X., Kumar, V., Tsai, N.-P., and Auerbach, B.D. (2022). Hyperexcitability and homeostasis in fragile X syndrome. Front Mol Neurosci *14*, 805929. DOI: 10.3389/fnmol.2021.805929.

Liu, Y.-J., Spangenberg, E.E., Tang, B., Holmes, T.C., Green, K.N., and Xu, X. (2021). Microglia elimination increases neural circuit connectivity and activity in adult mouse cortex. J Neurosci *41*, 1274–1287. DOI: 10.1523/JNEUROSCI.2140-20.2020.

Liu, Y.U., Ying, Y., Li, Y., Eyo, U.B., Chen, T., Zheng, J., Umpierre, A.D., Zhu, J., Bosco, D.B., Dong, H., et al. (2019). Neuronal network activity controls microglial process surveillance in awake mice via norepinephrine signaling. Nat Neurosci *22*, 1771–1781. DOI: 10.1038/s41593-019-0511-3.

Liu, Z.-W., Faraguna, U., Cirelli, C., Tononi, G., and Gao, X.-B. (2010). Direct evidence for wake-related increases and sleep-related decreases in synaptic strength in rodent cortex. J Neurosci *30*, 8671–8675. DOI: 10.1523/JNEUROSCI.1409-10.2010.

Lovelace, J.W., Ethell, I.M., Binder, D.K., and Razak, K.A. (2018). Translation-relevant EEG phenotypes in a mouse model of Fragile X Syndrome. Neurobiol Dis *115*, 39–48. DOI: 10.1016/j.nbd.2018.03.012.

Lu, H.-C., Pollack, H., Lefante, J.J., Mills, A.A., and Tian, D. (2019). Altered sleep architecture, rapid eye movement sleep, and neural oscillation in a mouse model of human chromosome 16p11.2 microdeletion. Sleep *42*, zsy253. DOI: 10.1093/sleep/zsy253.

Maccarrone, M., Rossi, S., Bari, M., De Chiara, V., Rapino, C., Musella, A., Bernardi, G., Bagni, C., and Centonze, D. (2010). Abnormal mGlu 5 receptor/endocannabinoid coupling in mice lacking FMRP and BC1 RNA. Neuropsychopharmacol *35*, 1500–1509. DOI: 10.1038/npp.2010.19.

Maenner, M.J., Shaw, K.A., Baio, J., Washington, A., Patrick, M., DiRienze, M., Christensen, D.L., Wiggins, L.D., Pettygrove, S., Andrews, J.G., et al. (2020). Prevalence of autism spectrum disorder among children aged 8 years — Autism and developmental disabilities monitoring network , 11 sites , United States , 2016. MMWR Surveill Summ *69*, 1–12. DOI: http://dx.doi.org/10.15585/mmwr.ss6904a1external icon.

McFarlane, H.G., Kusek, G.K., Yang, M., Phoenix, J.L., Bolivar, V.J., and Crawley, J.N. (2008). Autism-like behavioral phenotypes in BTBR T+tf/J mice. Genes Brain Behav *7*, 152–163. DOI: 10.1111/j.1601-183X.2007.00330.x.

Meyza, K.Z., and Blanchard, D.C. (2017). The BTBR mouse model of idiopathic autism – Current view on mechanisms. Neurosci Biobehav R *76*, 99–110. DOI: 10.1016/j.neubiorev.2016.12.037.

Nelson, S.B., and Valakh, V. (2015). Excitatory/inhibitory balance and circuit homeostasis in autism spectrum disorders. Neuron *87*, 684–698. DOI: 10.1016/j.neuron.2015.07.033.

Oliet, S.H., Piet, R., and Poulain, D.A. (2001). Control of glutamate clearance and synaptic efficacy by glial coverage of neurons. Science *292*, 923–926. DOI: 10.1126/science.1059162.

Paolicelli, R.C., Bolasco, G., Pagani, F., Maggi, L., Scianni, M., Panzanelli, P., Giustetto, M., Ferreira, T.A., Guiducci, E., Dumas, L., et al. (2011). Synaptic pruning by microglia is necessary for normal brain development. Science *333*, 1456–1458. DOI: 10.1126/science.1202529.

Paukert, M., Agarwal, A., Cha, J., Doze, V.A., Kang, J.U., and Bergles, D.E. (2014).

Norepinephrine controls astroglial responsiveness to local circuit activity. Neuron *82*, 1263–1270. DOI: 10.1016/j.neuron.2014.04.038.

Pretzsch, C.M., Freyberg, J., Voinescu, B., Lythgoe, D., Horder, J., Mendez, M.A., Wichers, R., Ajram, L., Ivin, G., Heasman, M., et al. (2019). Effects of cannabidiol on brain excitation and inhibition systems; a randomised placebo-controlled single dose trial during magnetic resonance spectroscopy in adults with and without autism spectrum disorder. Neuropsychopharmacology *44*, 1398–1405. DOI: 10.1038/s41386-019-0333-8.

Qin, M., Zeidler, Z., Moulton, K., Krych, L., Xia, Z., and Smith, C.B. (2015). Endocannabinoid-mediated improvement on a test of aversive memory in a mouse model of fragile X syndrome. Behav Brain Res *291*, 164–171. DOI: 10.1016/j.bbr.2015.05.003.

Robertson, C.E., and Baron-Cohen, S. (2017). Sensory perception in autism. Nat Rev Neurosci *18*, 671–684. DOI: 10.1038/nrn.2017.112.

Rubenstein, J.L.R., and Merzenich, M.M. (2003). Model of autism : Increased ratio of excitation / inhibition in key neural systems. Genes Brain Behav *2*, 255–267. DOI: 10.1046/j.1601-183X.2003.00037.x.

Sabanov, V., Braat, S., D'Andrea, L., Willemsen, R., Zeidler, S., Rooms, L., Bagni, C., Kooy, R.F., and Balschun, D. (2017). Impaired GABAergic inhibition in the hippocampus of Fmr1 knockout mice. Neuropharmacology *116*, 71–81. DOI: 10.1016/j.neuropharm.2016.12.010.

Saré, R.M., Harkless, L., Levine, M., Torossian, A., Sheeler, C.A., and Smith, C.B. (2017). Deficient sleep in mouse models of fragile X syndrome. Front Mol Neursci *10*, 280. DOI: 10.3389/fnmol.2017.00280.

Saré, R.M., Lemons, A., Song, A., and Smith, C.B. (2021). Sleep duration in mouse models of neurodevelopmental disorders. Brain Sci *11*, 0–7. DOI: 10.3390/brainsci11010031.

Sawicka, K., Hale, C.R., Park, C.Y., Fak, J.J., Gresack, J.E., Van Driesche, S.J., Kang, J.J., Darnell, J.C., and Darnell, R.B. (2019). FMRP has a cell-type-specific role in CA1 pyramidal neurons to regulate autism- related transcripts and circadian memory. Elife *8*, e46919. DOI: 10.7554/eLife.46919.

Schreck, K.A., and Richdale, A.L. (2020). Sleep problems, behavior, and psychopathology in autism: inter-relationships across the lifespan. Curr Opin Psychol *34*, 105–111. DOI: 10.1016/j.copsyc.2019.12.003.

Seok, B.S., Bélanger-Nelson, E., Provost, C., Gibbs, S., and Mongrain, V. (2018). The effect of Neuroligin-2 absence on sleep architecture and electroencephalographic activity in mice. Mol Brain *11*, 1–11. DOI: 10.1186/s13041-018-0394-3.

Shigetomi, E., Tong, X., Kwan, K.Y., Corey, D.P., and Khakh, B.S. (2012). TRPA1 channels regulate astrocyte resting calcium and inhibitory synapse efficacy through GAT-3. Nat Neurosci *15*, 70–80. DOI: 10.1038/nn.3000.

Sinclair, D., Featherstone, R., Naschek, M., Nam, J., Du, A., Wright, S., Pance, K., Weger, R., Akuzawa, S., Matsumoto, M., et al. (2017). GABA-B agonist baclofen normalizes auditory-evoked neural oscillations and behavioral deficits in the Fmr1 knockout mouse model of Fragile X syndrome. ENeuro *4*, 1–13. DOI:

Speed, H.E., Masiulis, I., Gibson, J.R., and Powell, C.M. (2015). Increased cortical inhibition in autism-linked neuroligin-3R451C mice is due in part to loss of endocannabinoid signaling. PLoS One *10*, e0140638. DOI: 10.1371/journal.pone.0140638.

Stowell, R.D., Sipe, G.O., Dawes, R.P., Batchelor, H.N., Lordy, K.A., Whitelaw, B.S., Stoessel, M.B., Bidlack, J.M., Brown, E., Sur, M., et al. (2019). Noradrenergic signaling in the wakeful state inhibits microglial surveillance and synaptic plasticity in the mouse visual cortex. Nat Neurosci *22*, 1782–1792. DOI: 10.1038/s41593-019-0514-0.

Tabuchi, K., Blundell, J., Etherton, M.R., Hammer, R.E., Liu, X., Powell, C.M., and Südhof, T.C. (2007). A neuroligin-3 mutation implicated in autism increases inhibitory synaptic transmission in mice. Science *318*, 71–76. DOI: 10.1126/science.1146221.

Thomas, A.M., Schwartz, M.D., Saxe, M.D., and Kilduff, T.S. (2017). Cntnap2 knockout rats and mice exhibit epileptiform activity and abnormal sleep-wake physiology. Sleep *40*, 1–14. DOI: 10.1093/sleep/zsw026.

Tran, T., Unal, C.T., Severin, D., Zaborszky, L., Rotstein, H.G., Kirkwood, A., and Golowasch, J. (2019). Ionic current correlations are ubiquitous across phyla. Sci Rep *9*, 1687. DOI: 10.1038/s41598-018-38405-6.

Tsuchiya, Y., Minami, Y., Umemura, Y., Watanabe, H., Ono, D., Nakamura, W., Takahashi, T., Honma, S., Kondoh, G., Matsuishi, T., et al. (2015). Disruption of MeCP2 attenuates circadian rhythm in CRISPR/Cas9-based Rett syndrome model mouse. Genes Cells *20*, 992–1005. DOI: 10.1111/gtc.12305.

Unichenko, P., Yang, J., Kirischuk, S., Kolbaev, S., Kilb, W., Hammer, M., Krueger-Burg, D., Brose, N., and Luhmann, H.J. (2018). Autism related neuroligin-4 knockout impairs intracortical processing but not sensory inputs in mouse barrel cortex. Cereb Cortex *28*, 2873–2886. DOI: 10.1093/cercor/bhx165.

Vyazovskiy, V. V, Cirelli, C., Pfister-Genskow, M., Faraguna, U., and Tononi, G. (2008). Molecular and electrophysiological evidence for net synaptic potentiation in wake and depression in sleep. Nat Neurosci *11*, 200–208. DOI: 10.1038/nn2035.

Wahlstrom-Helgren, S., and Klyachko, V.A. (2015). GABAB receptor-mediated feed-forward circuit dysfunction in the mouse model of fragile X syndrome. J Physiol *593*, 5009–5024. DOI: 10.1113/JP271190.

Wallace, M.L., Burette, A.C., Weinberg, R.J., and Philpot, B.D. (2012). Maternal loss of Ube3a produces an excitatory/inhibitory imbalance through neuron type-specific synaptic defects. Neuron *74*, 793–800. DOI: 10.1016/j.neuron.2012.03.036.

Wei, D., Dinh, D., Lee, D., Li, D., Anguren, A., Moreno-Sanz, G., Gall, C.M., and Piomelli, D. (2016). Enhancement of anandamide-mediated endocannabinoid signaling corrects autism-related social impairment. Cannabis Cannabinoid Res *1*, 81–89. DOI: 10.1089/can.2015.0008.

Wither, R.G., Colic, S., Wu, C., Bardakjian, B.L., Zhang, L., and Eubanks, J.H. (2012). Daily rhythmic behaviors and thermoregulatory patterns are disrupted in adult female MeCP2-deficient mice. PLoS One *7*, e35396. DOI: 10.1371/journal.pone.0035396.

Zhang, L., and Alger, B.E. (2010). Enhanced endocannabinoid signaling elevates neuronal excitability in fragile X syndrome. J Neurosci *30*, 5724–5729. DOI: 10.1523/JNEUROSCI.0795-10.2010.

Zhang, J., Fang, Z., Jud, C., Vansteensel, M.J., Kaasik, K., Lee, C.C., Albrecht, U., Tamanini, F., Meijer, J.H., Oostra, B.A., et al. (2008). Fragile X-related proteins regulate mammalian circadian behavioral rhythms. Am J Hum Genet *83*, 43–52. DOI: 10.1016/j.ajhg.2008.06.003.

Zhang, W., Peterson, M., Beyer, B., Frankel, W.N., and Zhang, Z. (2014). Loss of MeCP2 from

forebrain excitatory neurons leads to cortical hyperexcitation and seizures. J Neurosci *34*, 2754–2763. DOI: 10.1523/JNEUROSCI.4900-12.2014.

Zhao, J.-P., and Yoshii, A. (2019). Hyperexcitability of the local cortical circuit in mouse models of tuberous sclerosis complex. Mol Brain *12*, 1–13. DOI: 10.1186/s13041-019-0427-6.

Zhong, L.R., Chen, X., Park, E., Sudhof, T.C., and Chen, L. (2018). Retinoic acid receptor RAR alpha-dependent synaptic signaling mediates homeostatic synaptic plasticity at the inhibitory synapses of mouse visual cortex. J Neurosci *38*, 10454–10466. DOI: 10.1523/JNEUROSCI.1133-18.2018.

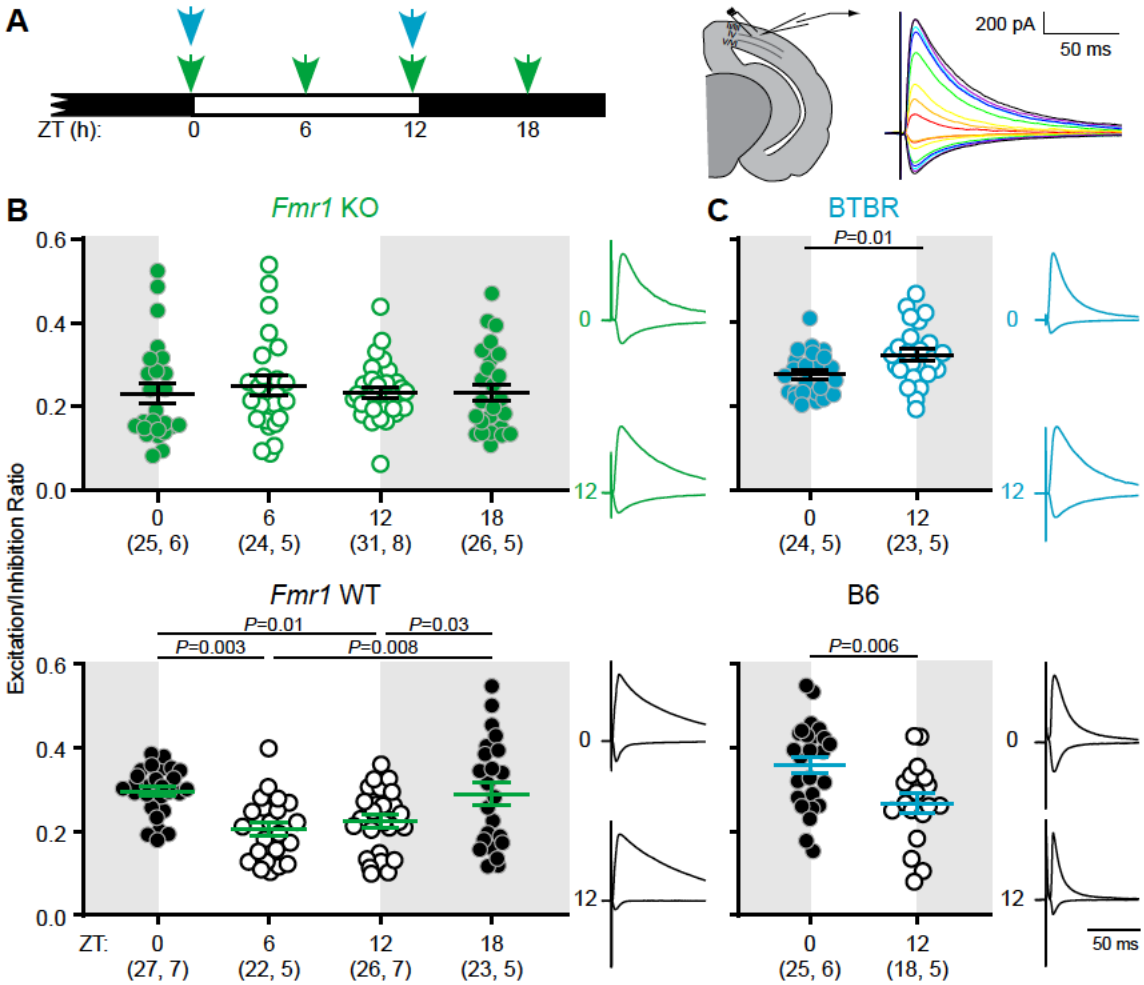

Figure 1. E/I is dysregulated in two mouse models of autism. (A) Left: *Fmr1* KO/WT (green) and BTBR/B6 (blue) mice were sacrificed at the indicated times of day. Right: Acute brain slices containing V1 were obtained, and responses to layer 2/3 stimulation over a range of intensities were recorded using whole-cell patch clamp of layer 2/3 pyramidal neurons. Inhibitory (upward deflection) and excitatory (downward deflection) responses were recorded in the same cell and the E/I ratio was calculated using the stimulation intensities over which the E/I ratio was stable (Bridi et al., 2020). (B) Oscillation of the E/I ratio across the day is absent in *Fmr1* KO mice. Top: *Fmr1* KO Kruskal-Wallis $H_{(3, 102)}$=1.62, P=0.65. Bottom: *Fmr1* WT 1-way ANOVA $F_{(3, 94)}$=6.67, P=0.0004; Holm-Sidak post-hoc test P values indicated. (C) BTBR mice exhibit a phase-shifted E/I oscillation, such that the E/I ratio is high at ZT12, contrasting with higher E/I at ZT0 in B6 mice. Top: BTBR 2-tailed t test $t_{(45)}$=2.64; Bottom: B6 2-tailed t test $t_{(41)}$=2.93. For all panels, sample size is indicated as (cells, mice). Error bars indicate mean±SEM. Example traces are normalized to peak inhibitory response.

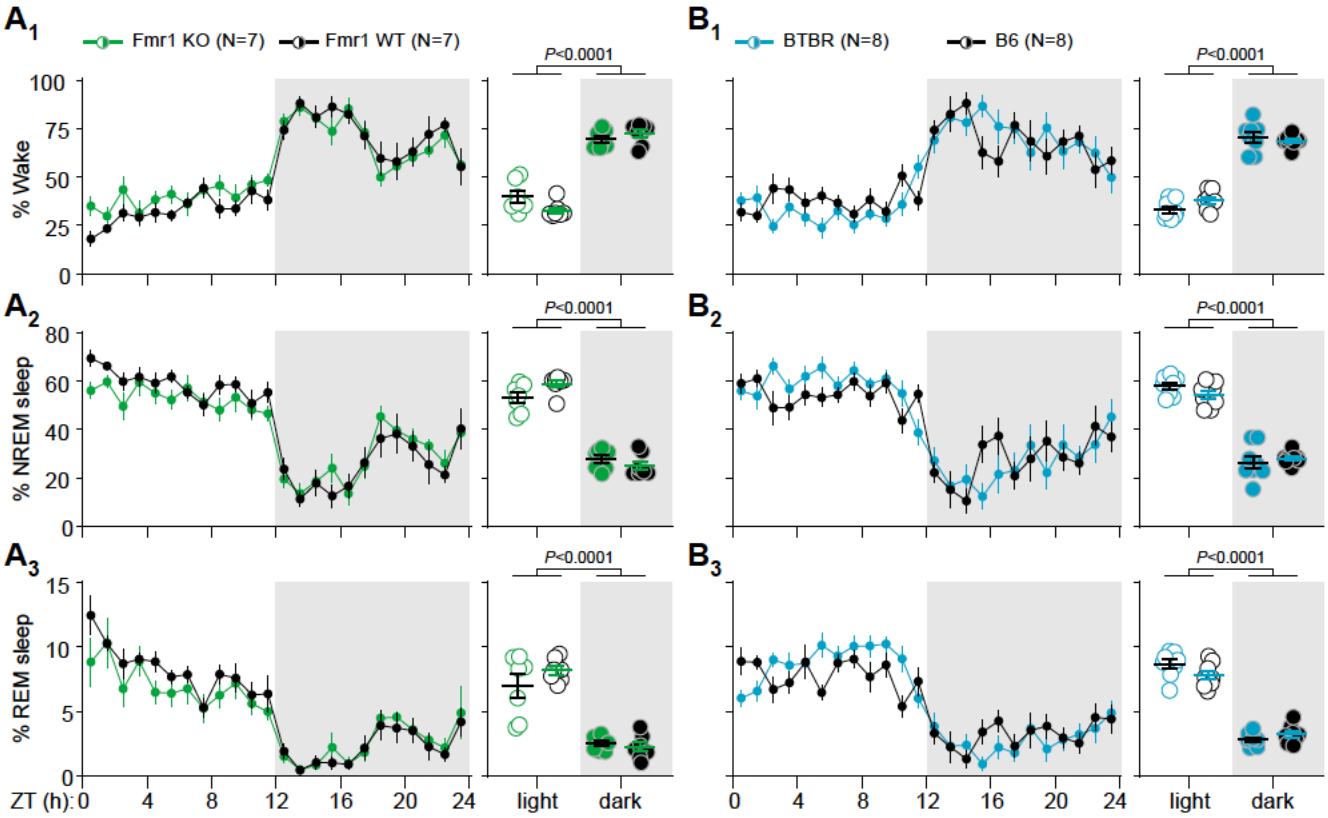

Figure 2. Sleep timing is normal in *Fmr1* KO and BTBR mice. (A) Percent time *Fmr1* mice spent awake (A_1), in NREM sleep (A_2), and in REM sleep (A_3). There was no significant main effect of genotype for any arousal state (%W $F_{(1, 12)}$=3.43, P=0.09, %NREM $F_{(1, 12)}$=2.80, P=0.12, %REM $F_{(1, 12)}$=0.86, P=0.37). There was also no significant genotype × time of day interaction when data were broken into 1h bins (left) (%W $F_{(23, 276)}$=0.88, P=0.63, %NREM $F_{(23, 276)}$=0.88, P=0.63, %REM $F_{(23, 276)}$=0.76, P=0.78) or averaged across the 12-h light and dark phases (right) (%W $F_{(1, 12)}$=3.12, P=0.10, %NREM $F_{(1, 12)}$=3.23, P=0.09, %REM $F_{(1, 12)}$=1.81, P=0.20). There was a significant main effect of time for all states (%W: $F_{(1, 12)}$=153.0, P<0.0001; %NREM: $F_{(1, 12)}$=162.9, P<0.0001; %REM: $F_{(1, 12)}$=85.6, P<0.0001). (B) Percent time BTBR and B6 mice spent in each arousal state. BTBR mice displayed grossly normal sleep timing (i.e. slept more during the dark phase) and there was no significant main effect of genotype for any arousal state (%W $F_{(1, 14)}$=0.72, P=0.41, %NREM $F_{(1, 14)}$=0.48, P=0.50, %REM $F_{(1, 14)}$=0.54, P=0.47). There were small but significant interaction effects for wake (B_1) and REM sleep (B_3) when data were broken into 1h bins (left) (%W $F_{(23, 322)}$=1.57, P=0.048, %NREM $F_{(23,322)}$=1.521, P=0.06, %REM $F_{(23, 322)}$=2.05, P=0.0035) and for REM sleep (B_3) when data were averaged into 12h bins (right) (%W $F_{(1, 14)}$=2.39, P=0.24, %NREM $F_{(1, 14)}$=1.95, P=0.18, %REM $F_{(1, 14)}$=4.93, P=0.04). There was a main time of day effect for all states (%W $F_{(1, 14)}$=258.9, P<0.0001, %NREM $F_{(1, 14)}$=232.0, P<0.0001, %REM $F_{(1, 14)}$=342.5, P<0.0001). Data were averaged over 3 recording days for each mouse prior to statistical analysis. All data were analyzed using 2-way repeated measures ANOVAs. Data are shown as mean ± SEM. N=number of mice.

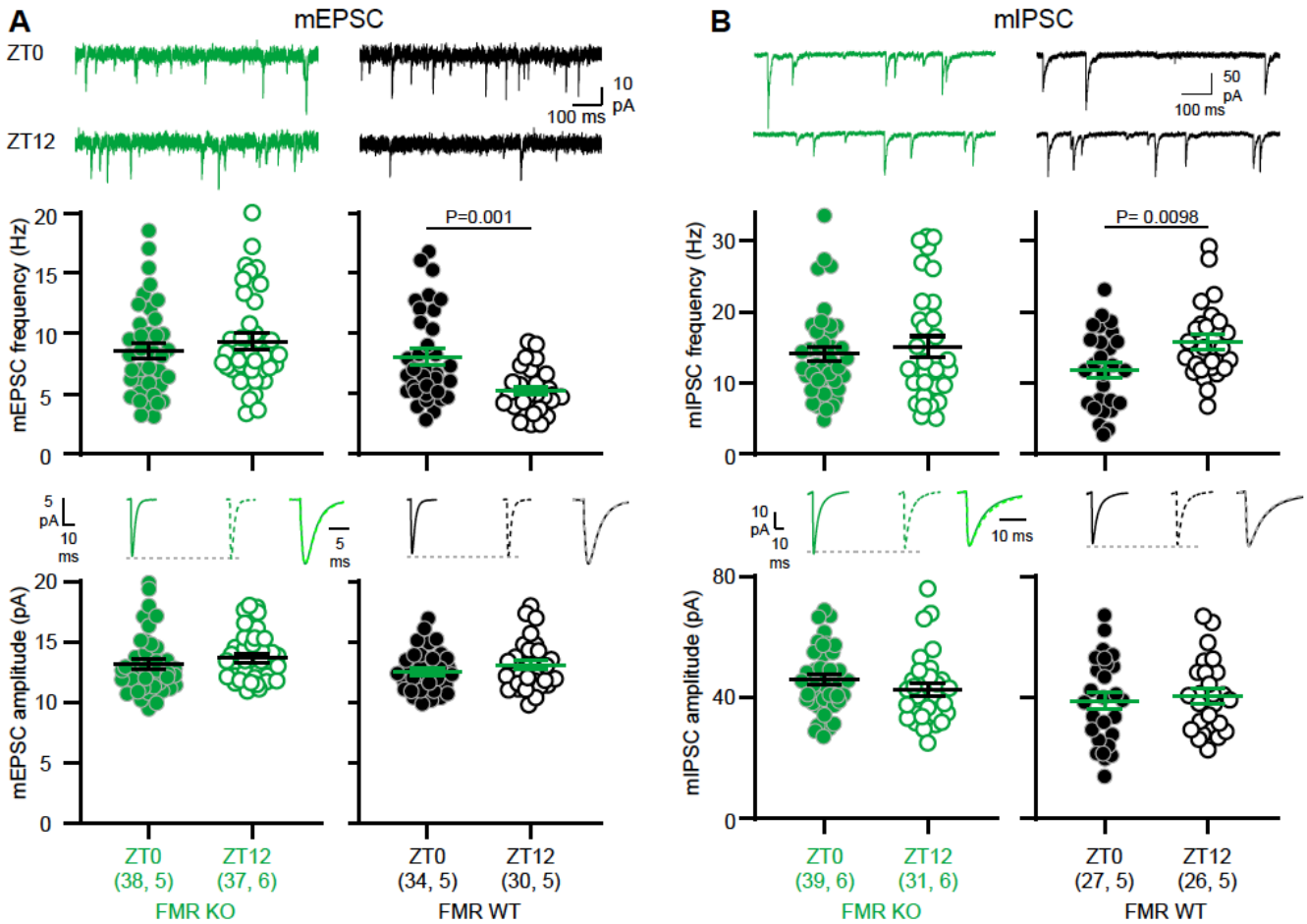

Figure 3. Oscillation of both excitation and inhibition is flattened in *Fmr1* KO mice. (A) mEPSC frequency does not change with time of day in *Fmr1* KO mice (U=613, P=0.35, Mann-Whitney test), but is higher at ZT0 in *Fmr1* WT control mice (U=269, P=0.001, Mann-Whitney test). Amplitude did not change with time of day in either genotype (KO: U=579, P=0.19; WT: U=445, P=0.39; Mann-Whitney test). (B) mIPSC frequency does not change with time of day in *Fmr1* KO mice (U=596, P=0.93, Mann-Whitney test), but is higher at ZT12 in *Fmr1* WT control mice ($t_{(51)}$=2.69, P=0.0098, t test). Amplitude did not change with time of day in either genotype (KO: $t_{(68)}$=1.26, P=0.21; WT: $t_{(51)}$=0.46, P=0.65, t test). Data are presented as mean±SEM. Sample size is indicated as (cells, mice). Averaged traces: solid lines indicate ZT0, dotted lines indicate ZT12; scaled, superimposed averaged traces illustrate that there was no difference in kinetics between the two times of day (Table S1).

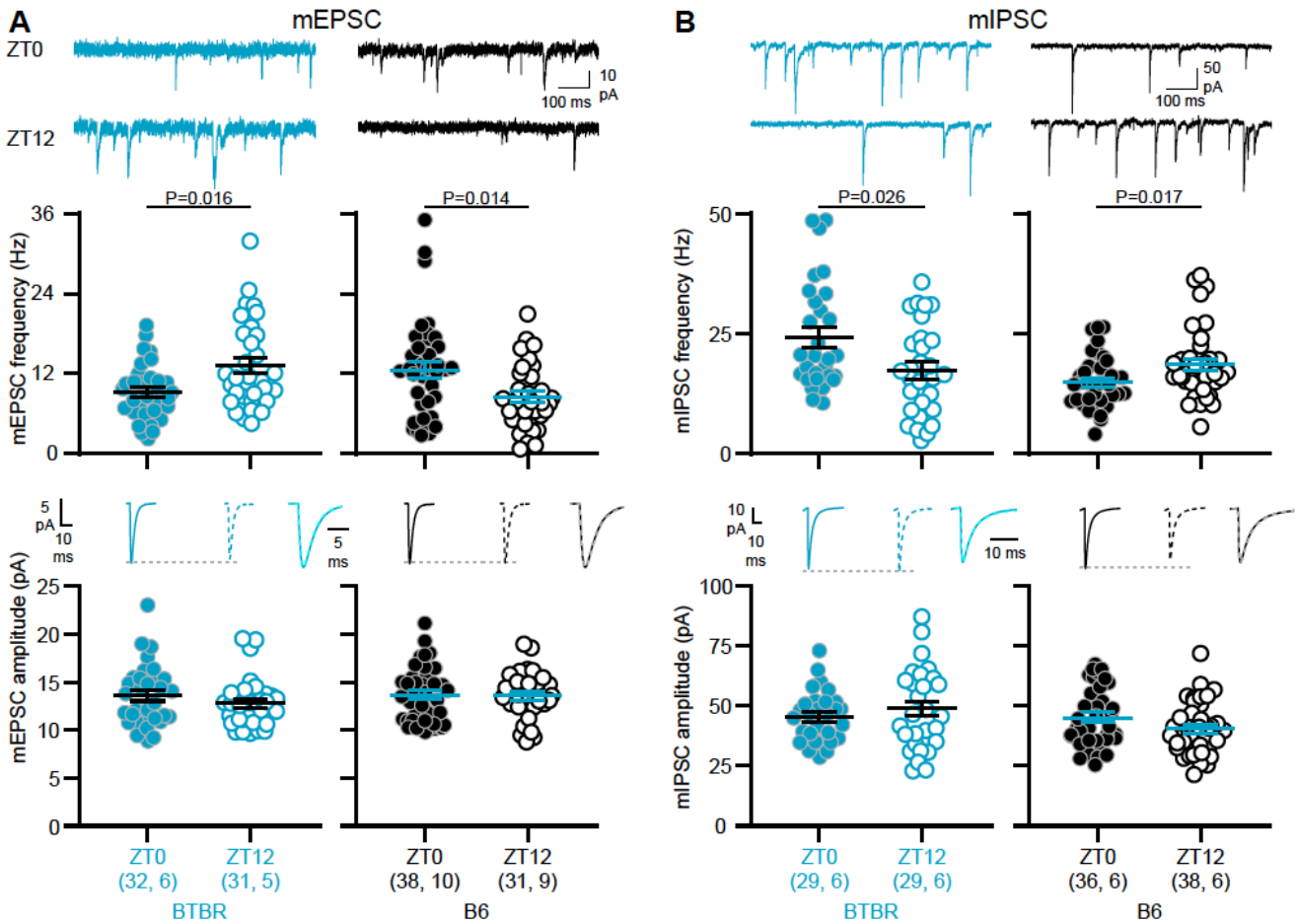

Figure 4. Oscillation of both excitation and inhibition is reversed in BTBR mice. (A) mEPSC frequency is higher at ZT12 in BTBR mice (U=322, P=0.016, Mann-Whitney test), and higher at ZT0 in B6 control mice ($t_{(67)}$=2.53, P=0.014, t test). Amplitude did not change with time of day in either genotype (BTBR: $t_{(61)}$=1.08, P=0.28; B6: $t_{(67)}$=0.11, P=0.91; t test). (B) mIPSC frequency is higher at ZT0 in BTBR mice (U=278, P=0.026, Mann-Whitney test), and higher at ZT12 in B6 controls (U=464, P=0.017, Mann-Whitney test). Amplitude did not change with time of day in either genotype (BTBR: $t_{(56)}$=0.93, P=0.36; B6: $t_{(72)}$=1.71, P=0.09, t test). Data are presented as mean±SEM. Sample size is indicated as (cells, mice). Averaged traces: solid lines indicate ZT0, dotted lines indicate ZT12; scaled, superimposed averaged traces illustrate that there was no difference in kinetics between the two times of day (Table S2).

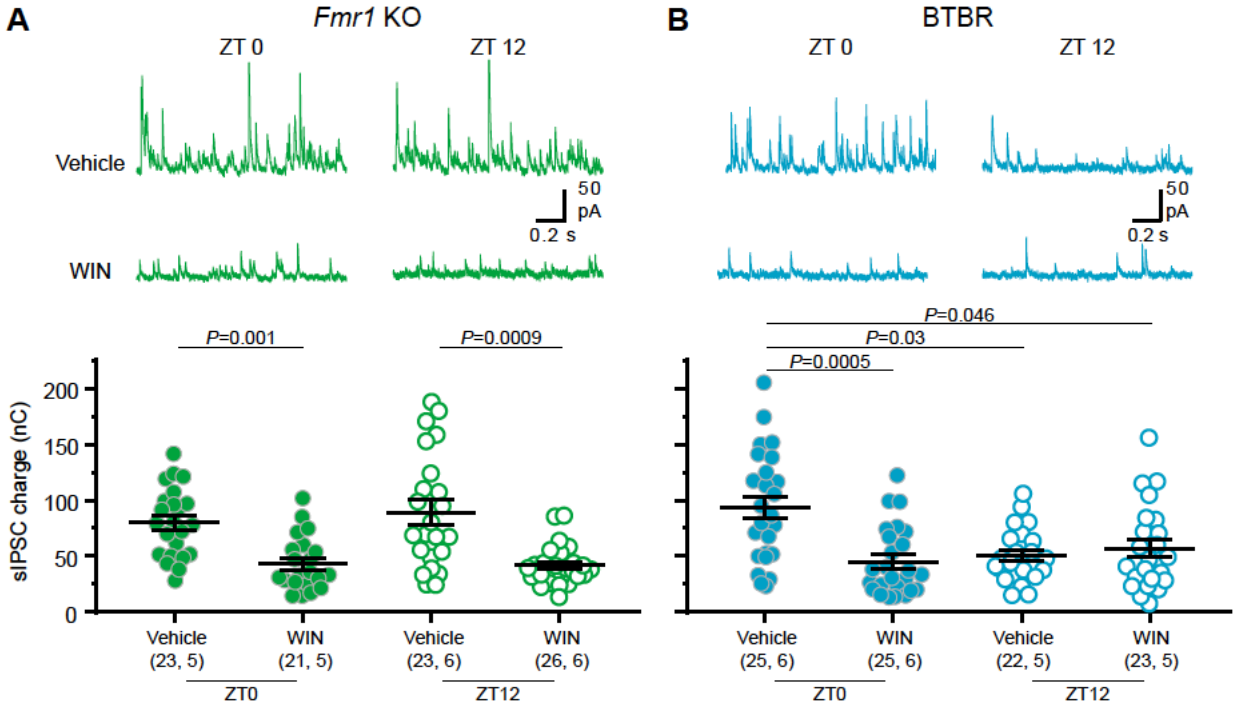

Figure 5. eCB signaling is dysregulated in *Fmr1* KO and BTBR mice. Slices were obtained at ZT0 or ZT12 and incubated in the eCB agonist WIN (10μM) or vehicle. sIPSCs were recorded from both treatment conditions in each animal. (A) Example traces (top) and quantification (bottom) of sIPSCs recorded from *Fmr1* KO slices. WIN significantly decreased sIPSC charge at both ZT0 and ZT12 (ANOVA on ranks H=28.73, P<0.0001; P values indicate significant differences according to Dunn's post-hoc test). sIPSC charge did not differ between times of day within vehicle or WIN treatment groups (P>0.9999). (B) Example traces (top) and quantification (bottom) of sIPSCs recorded from BTBR slices. WIN suppressed inhibitory transmission only at ZT0 (Kruskal-Wallis ANOVA on ranks H=16.9, P=0.0007; P values indicate significant differences between groups according to Dunn's post-hoc test). Data are shown as mean ±SEM and sample size is indicated as (cells, mice).

SUPPLEMENTARY TABLES.

Table S1. mE/IPSC characteristics in *Fmr1* KO and WT mice. Groups were compared using *t* tests or Mann-Whitney *U* tests, as indicated. Data are shown as mean ± SEM.

		Amplitude	Frequency	Rise	Decay	N
mEPSCs	KO ZT0	13.20 ± 0.4	8.55 ± 0.6	0.79 ± 0.01	2.53 ± 0.05	38 , 5
	KO ZT12	13.67 ± 0.3	9.35 ± 0.6	0.78 ± 0.02	2.63 ± 0.06	37 , 6
	test statistic	*U*=579	*U*=613	*U*=690	*U*=592.5	
	P	0.19	0.35	0.89	0.24	
	WT ZT0	12.58 ± 0.3	8.09 ± 0.6	0.77 ± 0.02	2.60 ± 0.05	34 , 5
	WT ZT12	13.09 ± 0.4	5.27 ± 0.3	0.77 ± 0.02	2.52 ± 0.06	30 , 5
	test statistic	*U*=445	*U*=269	$t_{(62)}$=0.23	*U*=415	
	P	0.39	**0.001***	0.82	0.2	
mIPSCs	KO ZT0	46.01 ± 1.7	14.09 ± 1.0	0.65 ± 0.03	5.58 ± 0.20	39 , 6
	KO ZT12	42.60 ± 2.1	15.17 ± 1.5	0.66 ± 0.03	6.37 ± 0.28	31 , 6
	test statistic	$t_{(68)}$=1.26	*U*=596	*U*=576	$t_{(68)}$=2.36	
	P	0.21	0.93	0.74	**0.02***	
	WT ZT0	38.80 ± 2.8	11.84 ± 1.1	0.75 ± 0.05	6.00 ± 0.33	27 , 5
	WT ZT12	40.47 ± 0.2	15.83 ± 1.0	0.69 ± 0.03	5.64 ± 0.20	26 , 5
	test statistic	$t_{(51)}$=0.46	$t_{(51)}$=2.69	*U*=330.5	$t_{(51)}$=0.94	
	P	0.65	**0.0098***	0.73	0.35	

Table S2. mE/IPSC characteristics in BTBR and B6 mice. Groups were compared using *t* tests or Mann-Whitney *U* tests, as indicated. Data are shown as mean ± SEM.

		Amplitude	Frequency	Rise	Decay	N
mEPSCs	BTBR ZT0	13.6 ± 0.6	9.2 ± 0.8	0.8 ± 0.03	2.7 ± 0.1	32 , 6
	BTBR ZT12	12.8 ± 0.5	13.2 ± 1.2	0.7 ± 0.02	2.5 ± 0.1	31 , 5
	test	*t*(61)=1.08	*U*=322	*t*(61)=1.49	*t*(61)=1.60	
	P	0.28	**0.016***	0.14	0.11	
	B6 ZT0	13.7 ± 0.5	12.5 ± 1.2	0.8 ± 0.03	2.8 ± 0.1	38 , 10
	B6 ZT12	13.6 ± 0.4	8.5 ± 0.9	0.8 ± 0.03	3.1 ± 0.1	31 , 9
	test	*t*(67)=0.91	*t*(67)=2.53	*U*=511	*U*=461.5	
	P	0.11	**0.014***	0.35	0.12	
mIPSCs	BTBR ZT0	45.6 ± 2.0	24.3 ± 2.2	0.5 ± 0.01	3.8 ± 0.1	29 , 6
	BTBR ZT12	49.0 ± 3.2	17.3 ± 1.8	0.5 ± 0.02	4.0 ± 0.2	29 , 6
	test statistic	*t*(56)=0.93	*U*=278	*t*(56)=0.27	*t*(56)=0.76	
	P	0.36	**0.026***	0.79	0.45	
	B6 ZT0	45.2 ± 2.1	14.9 ± 0.9	0.5 ± 0.02	4.2 ± 0.2	36 , 6
	B6 ZT12	40.6 ± 1.8	18.6 ± 1.2	0.6 ± 0.02	4.4 ± 0.2	38 , 6
	test statistic	*t*(72)=1.71	*U*=464	*t*(72)=1.82	*U*=648	
	P	0.09	**0.017***	0.07	0.70	

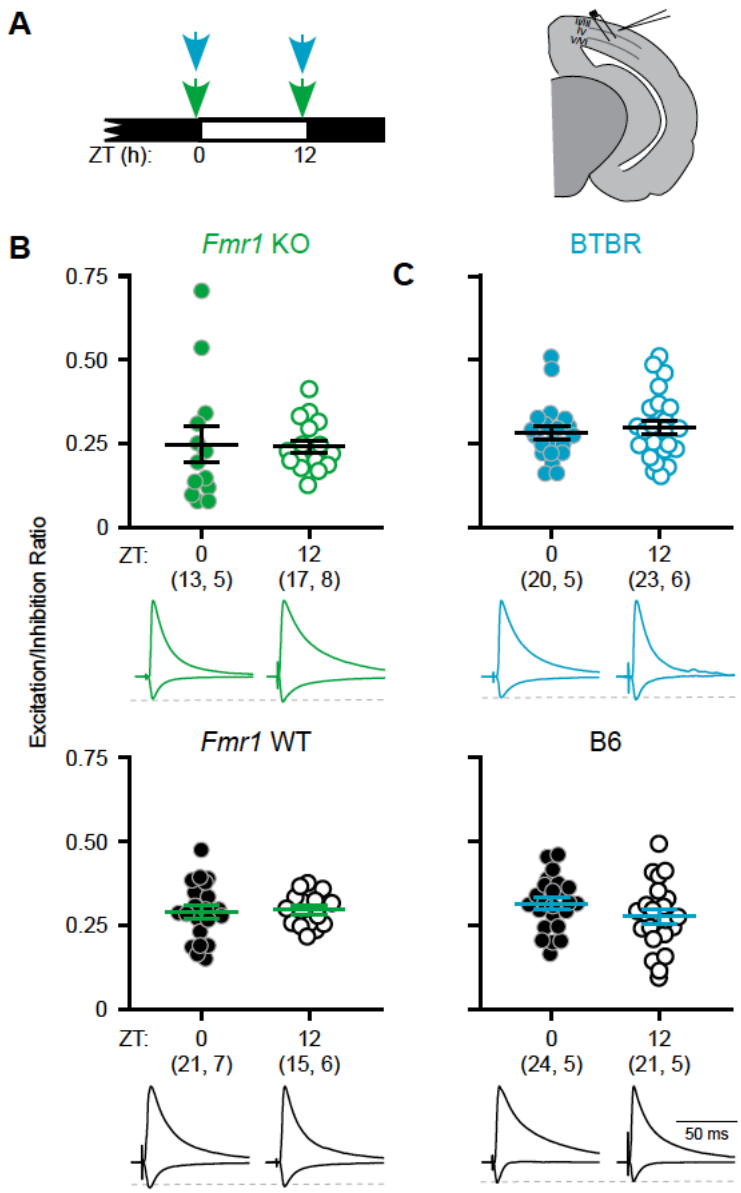

Supplementary Figure 1. The layer 4-2/3 E/I ratio is not affected by time of day. (A) *Fmr1* WT, *Fmr1* KO, B6, and BTBR mice were sacrificed at two times of day and acute brain slices containing V1 were collected for whole-cell patch clamp recordings of layer 2/3 pyramidal neurons in response to layer 4 stimulation. (B) The E/I ratio was not different between ZT0 and ZT12 in *Fmr1* KO and WT mice. Top: KO 2-tailed *t* test $t_{(28)}$=0.13, *P*=0.90. Bottom: WT 2-tailed *t* test $t_{(34)}$=0.22, *P*=0.82. When all groups were compared using a 2-way ANOVA, no significant main effect of time ($F_{(1, 62)}$=0.0002, *P*=0.99), genotype ($F_{(1, 62)}$=3.37, *P*=0.07), or time ´ genotype interaction ($F_{(1, 62)}$=0.05, *P*=0.82) was observed. (C) The E/I ratio was not different between ZT0 and ZT12 B6 and BTBR mice. Top: BTBR 2-tailed *t* test $t_{(41)}$=0.56, *P*=0.58. Bottom: B6 2-tailed *t* test $t_{(43)}$=1.44, *P*=0.16. When all groups were compared using a 2-way ANOVA, no significant main effect of time ($F_{(1, 84)}$=0.32, *P*=0.57), genotype ($F_{(1, 84)}$=0.08, *P*=0.78), or time ´ genotype interaction ($F_{(1, 84)}$=1.95, *P*=0.17) was observed. For all panels, sample size is indicated as (cells, mice). Error bars indicate mean±SEM Example traces show the inhibitory response (upward deflection) and excitatory response (downward deflection) in the same cell and are normalized to peak inhibitory response.

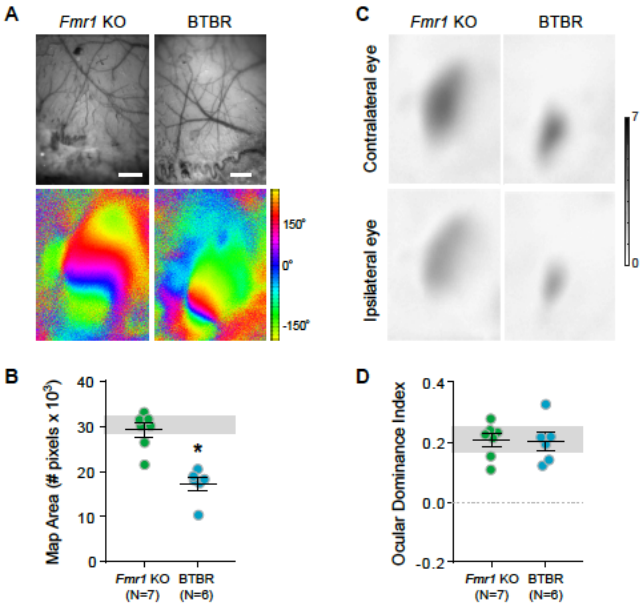

Supplementary Figure 2. V1 is functional and expresses normal ocular dominance bias in *Fmr1* KO and BTBR mice. **(A)** Example images of the cortical surface vasculature (top) and retinotopic maps (bottom) obtained by optical imaging of the intrinsic cortical signal while presenting a visual stimulus to the entire visual field of both eyes simultaneously. V1 of both mouse lines was functional and displayed retinotopic organization. **(B)** V1 size was normal in *Fmr1* KO mice but smaller in BTBR mice, compared with WT controls (shaded gray region indicates mean ± 95% CI of WT mice). Kruskal-Wallis ANOVA on ranks P=0.0011; *Fmr1* KO P>0.999, BTBR P=0.0007, Dunn's post-hoc test vs. WT). **(C)** Example images showing the response to each eye during presentation of a visual stimulus to the binocular visual field. **(D)** The ocular dominance index in binocular V1 was normal in both *Fmr1* KO and BTBR mice, compared to WT controls (shaded gray region indicates mean ± 95% CI of WT mice). ANOVA $F_{(2,\ 25)}$=0.014, P=0.986. Sample size is indicated as (# mice) and error bars represent SEM.

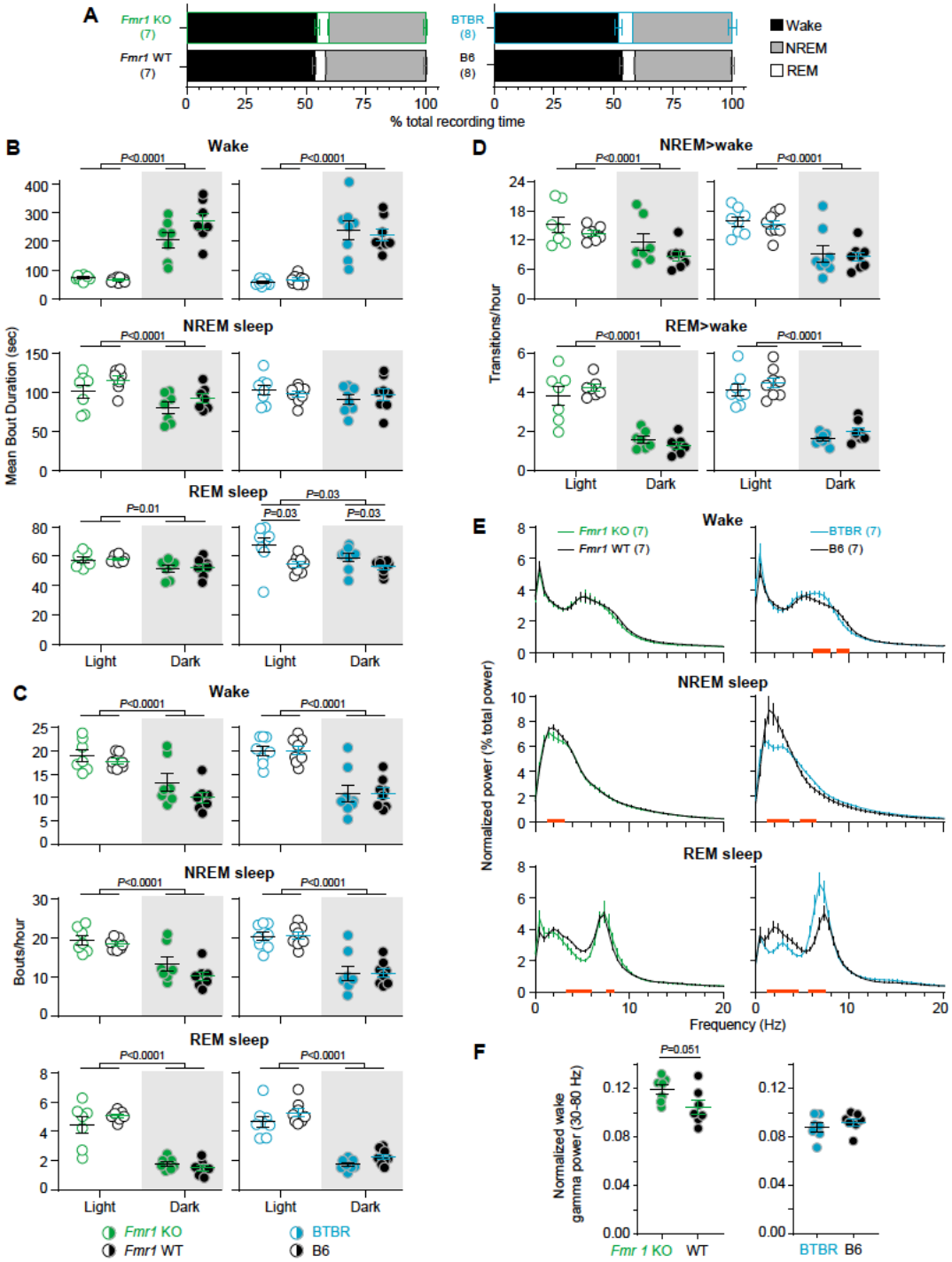

Supplementary Figure 3. Sleep architecture and EEG power in ASD model mice. **(A)** Overall amounts of wake, NREM sleep, and REM sleep did not differ between *Fmr1* KO and WT mice (wake: $t_{(12)}$=1.081, P=0.30; NREM: $t_{(12)}$=0.96, P=0.36, t test; REM: U=22, P=0.80, Mann-Whitney test), or between BTBR and B6 mice (wake: $t_{(14)}$=0.85, P=0.41; NREM: $t_{(14)}$=0.69, P=0.50; REM: $t_{(14)}$=0.73, P=0.48; t test).

B) In *Fmr1* mice, there was no effect of genotype or genotype × time interaction on bout duration for any arousal state (Wake: genotype $F_{(1,12)}$=2.67, P=0.13; interaction $F_{(1,12)}$=3.36, P=0.09; NREM: genotype $F_{(1,12)}$=2.14, P=0.17, interaction $F_{(1,12)}$=0.20, P=0.67; REM: genotype $F_{(1,12)}$=0.22, P=0.65, interaction $F_{(1,12)}$=0.004, P=0.95). Both *Fmr1* KO and WT mice had shorter wake and longer sleep bouts during the light phase (Wake: $F_{(1,12)}$=71.14, P<0.0001; NREM: $F_{(1,12)}$=61.80, P<0.0001; REM: $F_{(1,12)}$=9.41, P=0.01). BTBR mice had significantly longer REM sleep bouts than B6 mice in both the light and dark phases ($F_{(1,14)}$=6.05, P=0.03). There was also a main time of day effect for wake ($F_{(1,14)}$=71.78, P<0.0001) and REM ($F_{(1,14)}$=5.92, P=0.029) states. No genotype × time interactions were observed for any state (Wake: $F_{(1,14)}$=0.51, P=0.49; NREM: $F_{(1,14)}$=2.42, P=0.14; REM: $F_{(1,14)}$=2.54, P=0.13). All comparisons were conducted by 2-way repeated measures ANOVA. **(C)** Number of bouts/hour was higher for all arousal states during the light phase than during the dark phase (*Fmr1*: wake $F_{(1,12)}$=117.7, P<0.0001, NREM $F_{(1,12)}$=127.8, P<0.0001, REM $F_{(1,12)}$=92.6, P=0<0.0001; BTBR: wake $F_{(1,14)}$=117.2, P<0.0001, NREM $F_{(1,14)}$=135.4, P<0.0001, REM $F_{(1,14)}$=270.5, P<0.0001). No main effects of genotype (*Fmr1:* wake $F_{(1,12)}$=1.72, P=0.21, NREM $F_{(1,12)}$=1.66, P=0.22, REM $F_{(1,12)}$=0.31, P=0.59; BTBR wake $F_{(1,14)}$=0.0004, P=0.98, NREM $F_{(1,14)}$=0.005, P=0.94, REM $F_{(1,14)}$=3.34, P=0.09) or genotype × time interactions (*Fmr1:* wake $F_{(1,12)}$=2.25, P=0.16, NREM $F_{(1,12)}$=2.65, P=0.13, REM $F_{(1,12)}$=2.03, P=0.18; BTBR wake $F_{(1,14)}$= $1 \times 10^{-0.006}$, P=0.999, NREM $F_{(1,14)}$= 0.003, P=0.96, REM $F_{(1,14)}$=0.03, P=0.86) were observed. All comparisons were made using 2-way repeated measures ANOVAs. **(D)** The number of sleep-wake transitions per hour did not differ from WT in *Fmr1* KO (NREM>wake: $F_{(1,12)}$=1.62, P=0.23; REM>wake: $F_{(1,12)}$=0.05, P=0.83) or BTBR (NREM>wake: $F_{(1,14)}$=0.21, P=0.66; REM>wake: $F_{(1,14)}$=1.71, P=0.21) mice. There was no significant genotype-time interaction for either line (*Fmr1*: NREM>wake $F_{(1,12)}$=1.96, P=0.19; REM>wake $F_{(1,12)}$=1.45, P=0.25; BTBR: NREM>wake: $F_{(1,14)}$=2.5×10^{-5}, P=0.996; REM>wake: $F_{(1,14)}$=0.001, P=0.97). There were significant main time of day effects for both lines (*Fmr1*: NREM>wake $F_{(1,12)}$=107.7, P<0.0001; REM>wake $F_{(1,12)}$=75.7, P<0.0001; BTBR: NREM>wake: $F_{(1,14)}$=57.8, P<0.0001; REM>wake: $F_{(1,14)}$=246.1, P<0.0001). **(E-F)** Power spectra were calculated separately for wake, NREM sleep, and REM sleep arousal states and normalized to total spectral power (0.5-80 Hz) within that state. **(E)** Orange lines indicate the frequencies at which genotypes are significantly different (2-way ANOVA, Holm-Sidak post-hoc test P<0.05). **(F)** Wake power in the gamma range showed a strong trend toward higher power in *Fmr1* KO than WT controls ($t_{(12)}$=2.17, P=0.051). There was no difference between B6 and BTBR mice ($t_{(12)}$=0.92, P=0.38). For all panels, sample size is indicated as (mice) and bars represent mean ± SEM.

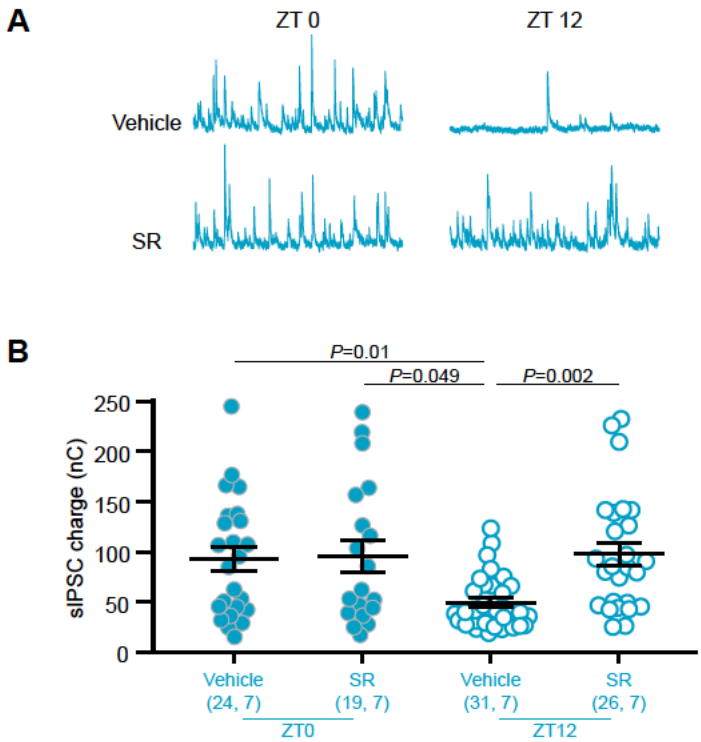

Supplementary Figure 4. eCB signaling is phase-shifted in BTBR mice. Acute brain slices containing V1 were obtained at ZT0 and ZT12, and sIPSCs in layer 2/3 pyramidal cells were recorded. (A) Example sIPSC traces. (B) Quantification of sIPSCs in the presence and absence of the eCB antagonist SR (10μM). SR enhances inhibitory transmission only during the light phase (Kruskal-Wallis ANOVA on ranks H=16.36, P=0.001; P values indicate significant differences between groups according to Dunn's post-hoc test). Sample size is indicated as (cells, mice) and bars represent mean ± SEM

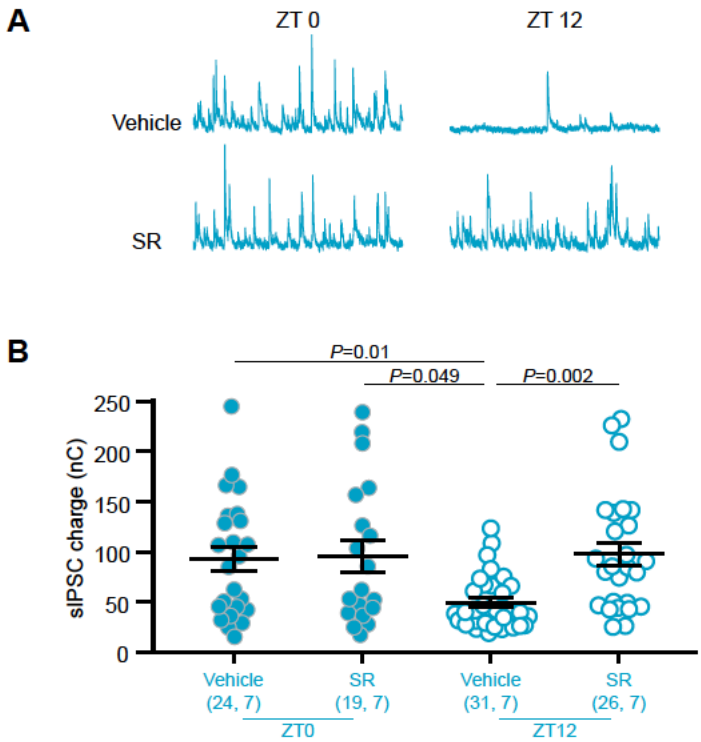

Supplementary Figure 4. eCB signaling is phase-shifted in BTBR mice. Acute brain slices containing V1 were obtained at ZT0 and ZT12, and sIPSCs in layer 2/3 pyramidal cells were recorded. (A) Example sIPSC traces. (B) Quantification of sIPSCs in the presence and absence of the eCB antagonist SR (10μM). SR enhances inhibitory transmission only during the light phase (Kruskal-Wallis ANOVA on ranks H=16.36, P=0.001; P values indicate significant differences between groups according to Dunn's post-hoc test). Sample size is indicated as (cells, mice) and bars represent mean ± SEM

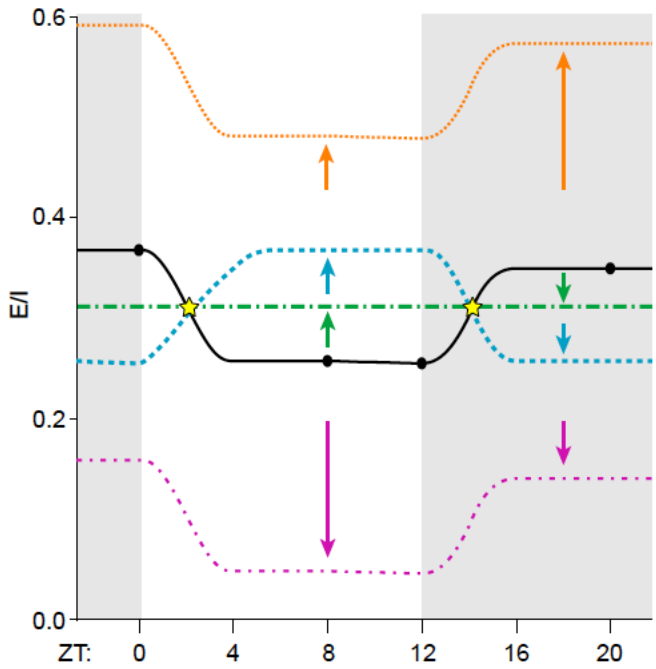

Supplementary Figure 5. Apparent differences in the E/I ratio between WT and ASD models can arise from multiple scenarios. In WT mice, E/I ratio oscillates over the 24h day (black; circles represent mean E/I ratio at four times of day as reported in (Bridi et al., 2020)). If the E/I ratio is measured at a single time of day and is observed to be altered in a genetic mouse model, several scenarios are possible. First, the oscillation could be intact, with the E/I ratio higher (orange) or lower (purple) at all times of day. Alternatively, the oscillation could be flattened (green) or shifted in time (blue), as observed in *Fmr1* KO and BTBR mice, respectively. Both of these scenarios would result in an apparent increase or decrease in the E/I ratio, depending on the time of day it is measured. Moreover, in these scenarios, there are two times of day when the E/I ratio is equal between WT and ASD model mice (yellow stars).